ELECTROFORMED NANOCRYSTALLINE COATINGS: AN ADVANCED ALTERNATIVE TO HARD CHROMIUM ELECTROPLATING

FINAL REPORT

2003-11-21

Subcontract Number: MTI-1418-01
For Research Services between McDermott Technology Inc., Babcock & Wilcox Canada and Integran Technologies Inc.

Our File No: 9903-DOD-NAN-0013

J.L. McCrea, M. Marcoccia and D. Limoges

Integran Technologies Inc., 1 Meridian Road, Toronto, Ontario M9W 4Z6 Canada

Report Documentation Page

Form Approved
OMB No. 0704-0188

1. REPORT DATE	2. REPORT TYPE	3. DATES COVERED
21 NOV 2003		**00-00-2003 to 00-00-2003**

4. TITLE AND SUBTITLE	5a. CONTRACT NUMBER
Electroformed Nanocrystalline Coatings: An Advanced Alternative to Hard Chrome Electroplating ? Final Report	5b. GRANT NUMBER
	5c. PROGRAM ELEMENT NUMBER
6. AUTHOR(S)	5d. PROJECT NUMBER
	5e. TASK NUMBER
	5f. WORK UNIT NUMBER
7. PERFORMING ORGANIZATION NAME(S) AND ADDRESS(ES) **Integran Technologies Inc,1 Meridian Road,Toronto, Ontario M9W 4Z6 Canada,**	8. PERFORMING ORGANIZATION REPORT NUMBER
9. SPONSORING/MONITORING AGENCY NAME(S) AND ADDRESS(ES)	10. SPONSOR/MONITOR'S ACRONYM(S)
	11. SPONSOR/MONITOR'S REPORT NUMBER(S)

12. DISTRIBUTION/AVAILABILITY STATEMENT
Approved for public release; distribution unlimited

13. SUPPLEMENTARY NOTES

14. ABSTRACT

15. SUBJECT TERMS

16. SECURITY CLASSIFICATION OF:			17. LIMITATION OF ABSTRACT	18. NUMBER OF PAGES	19a. NAME OF RESPONSIBLE PERSON
a. REPORT **unclassified**	b. ABSTRACT **unclassified**	c. THIS PAGE **unclassified**	**Same as Report (SAR)**	**72**	

DISCLAIMER

ELECTROFORMED NANOCRYSTALLINE COATINGS: AN ADVANCED ALTERNATIVE TO HARD CHROMIUM ELECTROPLATING

2003-11-21

Subcontract Number: MTI-1418-01
Our File No: 9903-DOD-NAN-0013

Prepared by:

_____
J.L. McCrea
Team Leader, Nano Research

_____
M. Marcoccia
Applications Engineering Technologist

_____
D. Limoges
Applications Engineering Technologist

Reviewed by:

_____
F. Gonzalez
Manager Process and Product Development

Approved by:

_____
G. Palumbo
President & Chief Technical Officer

EXECUTIVE SUMMARY

This report is prepared as the final report for SERDP Project PP-1152, "Electroformed Nanocrystalline Coatings: An Advanced Alternative to Hard Chrome Electroplating" and covers the project activities from June 13th, 2000 to June 13th, 2003. The purpose of the project is to develop an environmentally benign, cost-effective replacement for hard chrome to be applied to non-line-of-sight-surfaces. The project incorporates electrodeposited nanocrystalline technology that produces materials with comparable performance to hard chrome. The report is organized into activities associated with Phases II and III of the project. Phase II optimizes the coating process and Phase III extends the process to complex internal diameter shapes. For each activity, the developmental process followed and experimental results obtained are presented. A summary of the process developed and current performance of the material as compared to hard chrome is presented.

In Phase I, three different alloy coatings were synthesized on a laboratory scale utilizing a designed experimental approach on the basis of previously developed intellectual property [1,2]. Binary alloys, Co-P and Co-Mo, were produced along with the ternary alloy, Co-Fe-P. These alloys were evaluated for grain size, hardness, coating thickness and thermal stability. Phase I also included effort to establish baseline emission, chemical waste production and process cost data.

In Phase II, a nanocrystalline cobalt-phosphorus alloy and associated process has been established, studied and optimized. Performance tests have been conducted on uncoated and coated samples (as well as reference materials) to establish properties and performance including: hardness (ASTM B578), ductility (ASTM B489), adhesion abrasive (Taber) wear (JIS H8503), sliding (pin-on-disk) wear (ASTM G99), (ASTM B571), electrochemical potentiodynamic polarization (ASTM G5), and salt spray (fog) corrosion (ASTM B117). Hydrogen embrittlement (ASTM F519) and constant amplitude axial fatigue (ASTM E466) tests were also performed.

As part of Phase III, the nanocrystalline cobalt-phosphorus alloy coating was applied to internal diameter surfaces. Anode selection and plating parameters were selected and tested on mock-ups designed to simulate the typical internal diameter surfaces encountered in DOD applications. As a final demonstration, the coating process was applied to an ID surface of the shock strut of a landing gear component, provided courtesy of Messy-Dowty Aerospace.

TABLE OF CONTENTS

TABLE OF FIGURES

LIST OF TABLES

ELECTROFORMED NANOCRYSTALLINE COATINGS: AN ADVANCED ALTERNATIVE TO HARD CHROME ELECTROPLATING

1.0 INTRODUCTION

In response to FY00 SERDP Statement of Need: "Alternative Technologies to Hard (Wet) Chrome Electroplating", McDermott Technology Inc. (MTI) in collaboration with Integran Technologies Inc. and B&W Canada initiated a project entitled: "Electroformed Nanocrystalline Coatings: An Advanced Alternative to Hard Chrome Electroplating" on June 13th, 2000. The objective of the program was to allow for the complete elimination of hexavalent chromium at rework, maintenance and manufacturing facilities within the DoD through the use of an advanced nanoscale coating. The approach, which was based upon electroplating, allows for the retention of numerous benefits associated with hard chrome coating technology (i.e., non-line-of-sight application, excellent coating adhesion, dimensional consistency and superior surface finish) and allows for the use of existing hard chrome plating infrastructure within the defence sector. This will significantly reduce the time and cost to practical implementation.

Hard chromium coatings (0.25 to 10 mil thick) are used extensively for imparting wear and erosion resistance to components in both industrial and military applications[3,4,5,6] because of their intrinsic high hardness (600-1000 VHN) and low friction coefficient (<0.2)[7]. Health risks associated with the use of hexavalent chromium baths, however, have been recognized since early 1930's[8] and, consequently, there is currently tremendous pressure to identify a commercially viable alternative to these hard chromium coatings.

In addition to the health risks associated with Cr^{6+}, there are several other process and performance drawbacks to hard chrome coatings. As a result of the relatively low electrolytic efficiency of Cr plating processes, deposition (or build) rates are relatively low compared to the plating of other metals and alloys (e.g., 1-2 mils per hour for Cr versus > 8 mils per hour for Nickel) [9]. Moreover, the intrinsic brittleness of hard chromium deposits (i.e., <0.1% tensile elongation [10]) invariably leads to micro or macro-cracked deposits. These 'cracks', which do not compromise wear and erosion resistance, are wholly unsuitable for applications where corrosion resistance is required. In these applications, an electrodeposited underlayer of more ductile and corrosion resistant material (usually Ni) must be applied [10].

From the above summary, it is apparent that a need exists for an alternative technology that: (a) meets the hardness and low coefficient of friction of hard chromium coatings, (b) significantly reduces environmental and health risks, and (c) provides process and performance improvements such as: i) increased deposition rates, ii)

enhanced ductility, and iii) improved spalling and corrosion resistance without the need of a nickel underlayer.

Electrodeposited nanocrystalline metal and alloy coatings, in addition to being fully compatible with current hard chromium plating infrastructure, have displayed properties that render them a superior alternative to hard chromium coating technology. In this light, a Cobalt-based nanostructured alloy was developed in this program as an environmentally benign replacement for hard chrome electroplating for Non-line-of-sight (NLOS) applications.

The technical objective of this program was to develop and optimize an advanced nanoscale coating technology based upon modification of environmentally-benign conventional electroplating (wet) techniques that yield coatings that meet or exceed the overall performance (hardness, wear, thermal stability) and life-cycle cost of existing hard (engineering) chromium electroplating. The program was divided into three phases: Technology Viability, Coating Optimization and Extension to Complex Shapes. This report only briefly summarizes the work performed in each phase, as the results in each phase are extensively reported in the annual reports. The main focus of this report is to provide a detailed account of the process and properties of the final optimized nanostructured coating selected as the most promising replacement for hard chrome electroplating: cobalt 2-3wt%phosphorus.

1.1 PHASE I

In Phase I three different alloy coatings were synthesized on a laboratory scale utilizing a designed experimental approach on the basis of previously developed intellectual property [11,12]. Binary alloys, Co-P and Co-Mo, were produced along with the ternary alloy, Co-Fe-P. These alloys were evaluated for grain size, hardness, coating thickness and thermal stability. Phase I also included effort to establish baseline emission, chemical waste production and process cost data. Criteria were established for each parameter and a go-no/go recommendation was made to proceed with the optimization of the ternary alloy, Co-Fe-P, based on the encouraging results of Phase I.

1.2 PHASE II

The objective of Phase II was to optimize the deposition process of the nanocrystalline Co-Fe-P alloy system and prepare samples for material property and performance tests. Mechanical tests investigated included hardness, ductility, adhesion and coefficient of friction. Performance tests include fatigue, corrosion, hydrogen embrittlement and wear. Because both corrosion and wear tests are critical to the performance of the coating, the optimization program included comparison tests of various compositions for wear (as reflected by the Taber abrasive test) and for resistance to salt fog environment. Phase II results indicated that nanocrystalline Co-P alloys have

the best corrosion performance, good sliding wear performance (pin-on-disk), but marginal abrasive (Taber) wear performance. Alternatively, Co-Fe-P has good wear performance (both abrasive and sliding), but poor corrosion performance. Additional development was performed to include Zn to the alloy to improve the corrosion performance while maintaining acceptable wear performance. While the abrasive and sliding wear of Co-Fe-Zn-P alloys was acceptable, salt-spray corrosion tests indicated no improvement in corrosion performance. Based on the results of the mechanical and performance tests, nanocrystalline Co-P was identified as the alloy with the most suitable properties for chrome replacement on ID surfaces to be further developed in Phase III.

1.3 PHASE III

In Phase III further studies were performed on the binary Co-P alloy system to specifically optimize the deposition process for various internal diameter geometries. Four different ID geometries commonly hard chrome plated in the aerospace industry, were identified and constructed. Nanocrystalline Co-P deposition on the ID's of these parts was demonstrated to a thickness of 0.002 and 0.010 inches.

2.0 PROCESS

Relying on previously developed intellectual property [11,12], nanocrystalline cobalt-phosphorus alloys were produced using pulsed current electrodeposition. The effect of various electrodeposition parameters (e.g. bath composition, pH, temperature, overpotential, bath additives, etc.) on the structure and properties of the deposits were investigated, modified and optimized to yield deposits with average grain sizes between 5 and 15nm. The volume of the plating tanks used for the study ranged from 2 litres to 50 litres. Plating baths larger than 20 litres were filtered using 1 to 20µm polystyrene filter cartridges, were mechanically stirred using impellers and were heated using immersion heaters with temperature controllers. Plating bath between 2 and 3.5 litres were not filtered, were mechanically stirred using magnetic stir bars and were heated using heating bands on the outside of the Pyrex kettles. Reagent grade chemicals and distilled water was used for all plating solutions. The majority of the samples were produces using consumable anodes (cobalt pieces in a titanium basket). However, for some smaller ID plating trials, non-consumable graphite anodes were successfully utilized. As will be shown in the following sections, the optimized bath chemistry and plating conditions for the process provides an overall plating efficiency is approximately 90% (see section 2.4), with a deposition rate ranging from 2 to 8 mils/hour, depending on current density.

2.1 BATH CHEMISTRY

2.1.1 Chloride/Orthophosphoric Acid Based Bath Chemistry

Nanocrystalline cobalt-phosphorus electrodeposits developed during the course this program were produced from a chloride/orthophosphoric based bath chemistry. The bath chemistry and operating condition ranges for optimized Co-P coating deposition are outlined in Table 2-1. Specimens were typically deposited onto mild steel coupons that were cleaned and activated prior to plating. Standard cleaning and activation procedures used in the electroplating industry were found to provide adequate adhesion of the Co-P coating to both 4130 and mild steel in accordance with in ASTM Standard B571-91. Table 2-2 shows the cleaning and activation procedure employed using commercially available alkaline cleaning solution (SOAK 5000) and hydrochloric acid.

Table 2-1 Chloride/Ortho-phosphoric acid based bath chemistry and process conditions to deposit nanocrystalline Co-P deposits.

Chemical	**Concentration Range**
Cobalt Chloride, $CoCl_2 \cdot 6H_2O$	150 – 250 g/L
Cobalt Carbonate, $CoCO_3$	0.05-2g/L
Ortho-phosphoric Acid, H_3PO_4	50 g/L
Phosphorous Acid, H_3PO_3	2 – 8 g/L
Plating Conditions	
T_{on}	2 ms
T_{off}	2 – 10 ms
$I_{average}$	150 – 250 mA/cm^2
pH	1.0 – 1.8
Temperature	70 – 85°C
Anode Material	Cobalt Pieces / Graphite
Cathode	AISI 1010 / AISI 4340

Table 2-2 Cleaning and Activation procedure for mild steel and 4130 steel prior to Co-P coating.

Step	**Current / Time / Temperature**
Alkaline Clean (10% SOAK5000)	Anodic 50mA/cm^2 5-10 minutes 65-85°C
Water Rinse 1	1 minute Room Temperature
Water Rinse 2	1 minute Room Temperature
Acid Pickel (25% HCl in water)	5-10 minutes Room Temperature

2.1.2 Co-Deposition of Hard Ceramic Particles (Boron Carbide, B_4C)

To further enhance the functionality of the coating it has been shown that hard ceramic particles can be co-deposited with the nanocrystalline Co-P coating, resulting in finely dispersed, well bonded hard ceramic particles in a nanocrystalline Co-P matrix. Using the typical bath chemistry and plating conditions outlined in Table 2-1, samples were deposited from solution containing boron carbide (B_4C) powder (with average particle size between 1 and 5µm) in concentrations up to 50 g/L. The resulting concentration of particulate in the deposits was found to be a function of concentration of particulate added to the plating solution, as shown in Figure 2-1. Variations in current density were not found to significantly affect the concentration particulate in the deposits. The cathodic current efficiency of the process was not found to be effectd by the co-deposition of the particles.

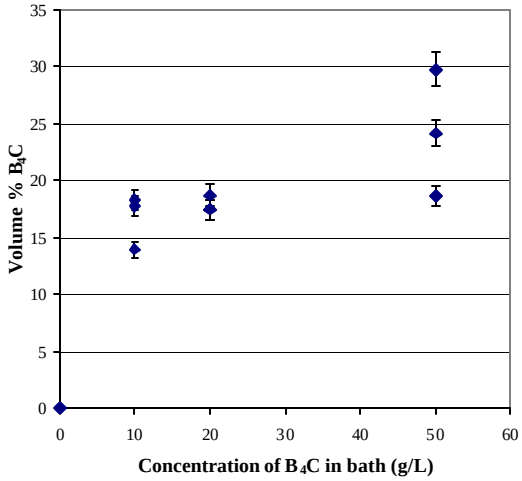

Figure 2-1 Concentration of B_4C particulate in the deposit as a function of B_4C particulate in the plating solution.

2.1.3 Electroplating Solution Control and Maintenance

Electroplating solution control and maintenance required for the solution described in section 2.1 is similar of that required for nickel-plating solutions. Ongoing maintenance procedures should include filtration and monitoring various solution parameters such as: pH, surface tension, and solution density. Filtration is required to control the presence of particles in the bath that can lead to surface imperfections in the coating. Monitoring the pH is essential in order to maintain deposit uniformity. Also, a rise in the pH above 2.0 will result in the formation of a pink precipitate in the solution significantly decreasing the quality of the deposit.

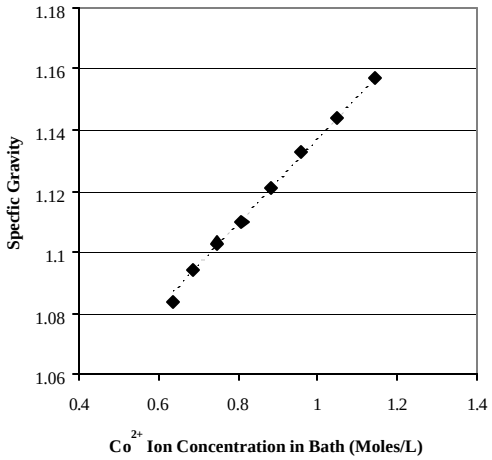

Figure 2-2 Specific gravity of the Co-P plating solution as a function of the molar concentration of Co^{2+} ions.

Rises in the pH were quite commonly observed due to excessive anode dissolution. A reduction in the pH occurs when a non-consumable anode is used. The pH of the solution should be lowered using concentrated hydrochloric acid and raised using cobalt carbonate. The surface tension of the solution should be maintained between 26 and 30 dynes/cm^2 using commercially available surfactants such as NPA-91. A surface tension in this range will help reduce the formation of pits and/or nodules on the deposit. Solution density should be monitored in order to maintain the cobalt ion concentration constant in the bath. Figure 2-2 shows the specific gravity of typical cobalt-phosphorous plating solution as a function of cobalt ion molar concentration in the bath. During plating, anode passivation and/or plating with a non-consumable anode will result in a decrease in the cobalt ion concentration in the solution. To maintain the optimal Co^{2+} ion concentration in the bath (0.75-1.15 Moles Co^{2+}) the specific gravity of the solution should be between 1.10 and 1.16.

Periodic maintenance procedures that may be necessary include activated carbon treatment/filtration and dummying. Activated carbon treatment/filtration will remove any organic impurities that may have accrued during the life of the bath that may be detrimental to the deposition process. Dummying (low current density plating) may be required to remove various metallic impurities in the plating solution (eg. Cu, Sn).

2.1.4 Efficiency

The effect of various pulse conditions and average current densities on the cathodic current efficiency of the cobalt-phosphorus electrodeposition process was studied. For this study Co-P was electrodeposited onto 4" x 1" mild steel coupons using the standard bath chemistry outlined in Table 2-1. Triplicate samples were pulse plated at 100, 150, 200 and 250 mA/cm^2 using a T_{on} of 2ms and a T_{off} of 0, 2, 4, 6 and 10ms. Samples were plated for a total of 15 minutes each. Each sample was weighed before and after deposition and the cathodic current efficiency was calculated. The total weight of the dendrites on each sample was also measured. Figure 2-3 plots the current efficiency as a function of pulse off time (T_{off}) for various current densities. In general the current efficiency was found to be between 75 and 95%, no trend was observed with increasing current density or increasing

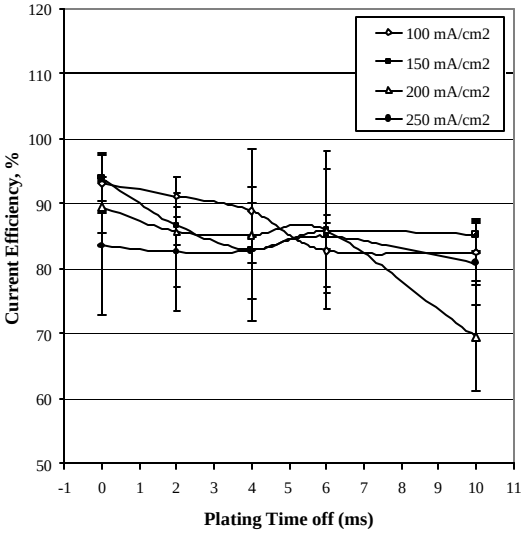

Figure 2-3 Cathodic current efficiency of Co-P electroplating as a function of pulse off time (T_{off}) for various average current densities.

pulse off time, with the exception of a slight decrease at a T_{off} of 10ms, which may be due to excessive dendrite formation due to the sharp edges of the test samples and the high peak current associated with the low duty cycle.

In Phase III, it was determined that for the case of ID plating the optimal pulse conditions were a T_{on} and T_{off} of 2 and 4 ms, respectively at an average current density of 150mA/cm^2. Using these pulse conditions the cathodic current efficiency was consistently calculated to be approximately 90%.

2.2 BATH STABILITY USING NON-CONSUMABLE GRAPHITE ANODE

Both consumable and non-consumable anodes can be used with the standard Co-P plating solution. However, due to the reactions at the anode during plating, the use of a non-consumable anode is only useful under certain conditions. While scaling-up the process to plate the ID of one-foot lengths of four-inch diameter pipe using non-consumable (graphite) anodes the consumption of phosphorous acid from the solution was higher than expected. One possible reaction that may explain the consumption is the oxidation of phosphorous acid to ortho-phosphorous acid. When using a non-consumable anode the anodic reactions are as follows:

$$2H_2O \rightarrow O_2 + 4H^+ + 4e^-$$
$$2Cl^-_{(aq)} \rightarrow Cl_{2(g)} + 2e^-$$

The evolution of oxygen at the anode is the predominant reaction, however, chlorine is also evolved as well, as noted by its distinct odour during plating. The following reaction is the likely oxidation reaction of phosphorous acid to ortho-phosphoric acid:

$$2(HO)_3P + O_2 \rightarrow 2(HO)_3PO \quad \text{or} \quad 2H_3PO_3 + O_2 \rightarrow 2H_3PO_4$$

The presence of chlorine in solution is believed to increase the rate of the above reaction, as chlorine is a strong oxidizer. Figure 2-4 shows the concentration of phosphorus in nanocrystalline Co-P deposits as a function of normalized plating time (in AmpHrs/Litre) for samples deposited using graphite anodes (two anode surface areas) and the ID of a 4" pipe, and a consumable cobalt anode. The rate of the decrease in the concentration of phosphorus in the deposit is much higher when a graphite anode is used over the consumable cobalt anode. This strongly indicates that the oxidation reaction is occurring when a graphite anode is employed. The oxidation rate was found to be higher when the anode surface area was higher (125cm^2 versus 30cm^2). For the case of the 4" ID plating run, the rate decrease is likely the highest as the combined anode current density and anode surface area were higher than the other tests. Another consequence of using non-consumable anodes is the depletion of Co^{2+} ions during plating. Figure 2-5 shows the change in solution density as a function of plating time for Co-P plating solution using both non-consumable and consumable anodes. The curves indicate that when using

non-consumable anodes, cobalt ions must be replenished in the bath in order to maintain the solution density constant.

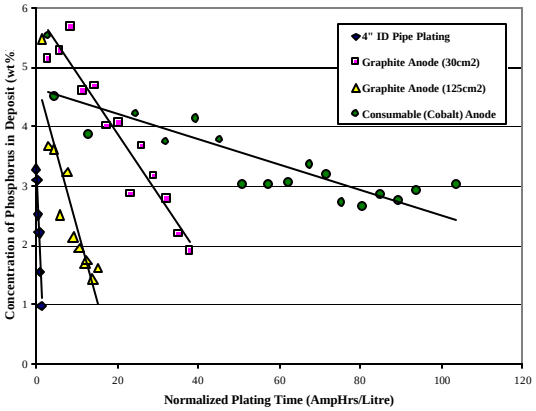

Figure 2-4 Concentration of phosphorus in the deposit as a function of normalized plating time (AmpHrs/Litre).

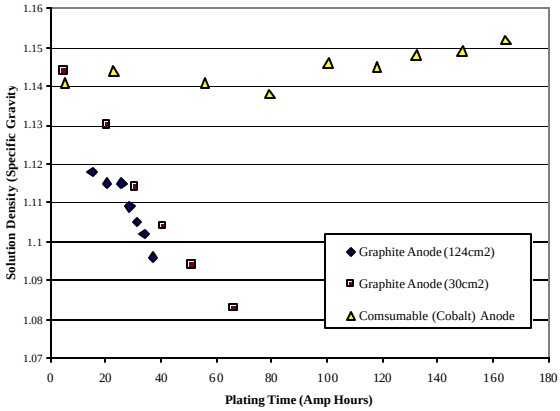

Figure 2-5 Specific gravity **(s**olution density) as a function of plating time (ampere hours) for nanocrystalline cobalt phosphorus deposits plated using graphite and cobalt anodes.

2.3 STRIPPING

2.3.1 Concentrated Nitric Acid

Concentrated nitric acid (specific gravity 1.42) was investigated as a stripping solution for Co-P plated on 4130 steel. Figure 2-6 shows the percentage of coating removed as a function of time for pure nitric acid and nitric acid with 0.008%(vol) hydrochloric acid. The removal rate was very fast, approximately 8 grams per hour, which corresponds to 225µm/hr (9mil/hr). The base metal (4130 steel) was found to be inert in the solution as the substrate lost less than 0.13% of its total weight after being immersed in the solution for 20 hours. Figure 2-7 shows the Co-P coating removal rate as a function of the total weight of dissolved coating per litre of nitric acid. From this curve it is seen that the removal rate slowly decreases with use but is relatively effective up until 80 grams have been dissolved in 1 litre of solution (dotted line on curve). After this point the solution starts to crystallize and becomes unstable and mildly aggressive towards the substrate.

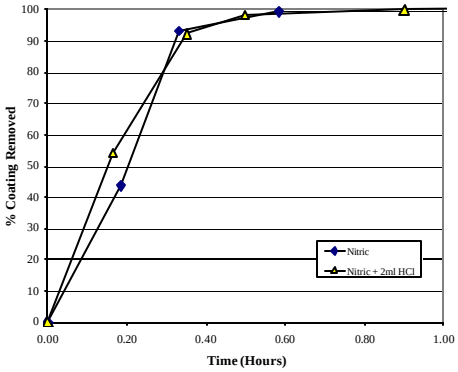

Figure 2-6 Percentage Co-P coating removed as a function of time in Nitric acid.

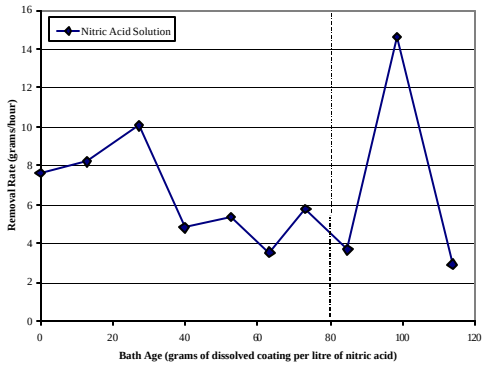

Figure 2-7 Co-P coating removal rate as a function of the total weight of dissolved coating per litre of nitric acid.

2.4 PROCESS COST

An estimate of the cost to electrodeposit various nanocrystalline Co-P alloys was performed using the hard chrome deposition process as a benchmark comparison. The cost was broken into two parts, the base metal cost and the power cost associated with the DC electrodeposition currents needed. As the hard chrome electrodeposition process uses a non-consumable anode, the base metal cost was estimated from the price of chromic acid. For the case of conventional nickel and nanocrystalline cobalt alloys, consumable anodes are used, thus the base metal price was estimated simply from the alloy composition. For the case of the phosphorus containing alloys, however, the cost of the hypo/phosphorous acid was included in the estimate. The cost analysis is given in Table 2-3.

The relative consumable cost for the nanocrystalline alloys is slightly higher than that for chrome due to the relatively high price of cobalt (~7US$/lb) and/or phosphorus. The relative power cost for the production of the nanocrystalline alloys, however, is far below that for chrome. This is due to two factors. First, hexavalent chrome ions need 6 electrons to be reduced to a metallic state at the cathode whereas both cobalt and iron only need 2 electrons. Therefore the chrome process requires 3 times as much electricity than the cobalt process. Secondly, the efficiency of the chrome process is significantly below that of the nanocrystalline alloy processes, further increasing the power cost. Therefore, estimating the cost of electricity at 0.1$/kWhr, the total relative process cost for the production of nanocrystalline Co and Co-3%P is 1.09 and 1.31, respectively, when compared to the hard chrome process. An additional factor that was not considered in the above cost analysis is the environmental costs associated with wastes generated during the process, and production costs, such as tank time can be quite substantial.

Table 2-3 Cost analysis for the production of electrodeposited nanocrystalline cobalt and cobalt-3%phosphorus compared to conventional nickel and hard chrome.

Plating Process	Nominal Plating Efficiency (%)	Consumables	Relative Plating Cost (by weight)	Relative Power Cost (by weight)	Total Relative Process Cost
Chrome(VI)	25	Cr_2O_3	1.00	1.00	1.00
Conventional Ni	90	Ni	0.70	0.08	0.44
Nano Co	>90	Co	1.83	0.08	1.09
Nano Co-3%P	>90	Co H_3PO_3	2.21	0.08	1.31

2.5 ENVIRONMENTAL IMPACT

With regard to potential environmental impact, it is anticipated that waste stream volumes will be, for all intents and purposes, identical to those currently experienced with hard chrome plating processes on a per tonne metal plated basis. However, the environmental impact of the wastes associated with the nanoscale deposition will be significantly reduced as none of the chemical constituents required for nanoscale cobalt-alloy deposition are presently on EPA and AFMC lists of hazardous materials. Moreover, the high plating efficiencies typically observed with nanoscale electrodeposition, are expected to significantly reduce overall electrical power requirements relative to that of chrome plating operations.

The potential impact on workplace safety was investigated by sampling the laboratory air directly above the plating tanks. The airborne emissions from three-nanocrystalline plating electrolytes (Co, Co-P and Co-Fe-P) were measured by sampling 30L of air over a 5 hour period during the electrodeposition process. A sampling line was placed about 1 inch from the surface of the plating solution and air was sampled at approximately 100mL/min. The vials were then analyzed for any traces of cobalt, iron, chloride, sulphate, and for two additives. A summary of the emission results is given in Table 2-4. The toxicity level given in the first column is that set by OSHA. In all cases the measured emissions were far below the toxicity level. For the case of the two additives, no emissions were measured above the background.

Table 2-4 Results from the emission analysis measurements for cobalt, cobalt-phosphorus and cobalt-iron-phosphorus bath chemistries.

Element/Compound	Toxicity Level[1] *(mg/m^3)*	Bath#1 Cobalt *(mg/m^3)*	Bath#2 Co-P *(mg/m^3)*	Bath#3 Co-Fe-P *(mg/m^3)*
Cobalt	0.05	0.0039	<0.0005	<0.0005
Iron	1.0	<0.0005	<0.0005	<0.0005
Chloride	N/A	0.216	0.043	0.053
Sulphate	N/A	0.258	0.014	0.29
Additive#1	N/A	N.A.B.	N.A.B.	N.A.B.
Additive#2	N/A	N.A.B.	N.A.B.	N.A.B.

[1]OSHA Time Weighted 8 Hr Avg, N.A.B. = Not Above Background

3.0 STRUCTURE

The surface morphology, deposit integrity and microstructure of the nanocrystalline Co-P deposits was characterized using optical microscopy, scanning electron microscopy (SEM), X-Ray diffraction (using Co k-α radiation, λ=1.7902 Angstroms) and transmission electron microscopy (TEM).

3.1 SURFACE MORPHOLOGY AND COATING INTEGRITY

Figure 3-1(a) is an optical micrograph (500x magnification) of a Co 2-3wt%P coating showing the surface morphology typically observed in nanocrystalline materials. The micrograph shows the "cauliflower" morphology typically observed in electrodeposited nanocrystalline materials. It should be noted that each "bump" in the structure is not a grain but rather a collection of thousands of much smaller grains. From this image it is also clear that no pits, pores or microcracks are present in the coating. Figure 3-1(b) shows a cross-section of a Co 2-3wt%P coating on the ID of a 1" diameter pipe, showing a 13 mil thick coating free of pores and/or cracks with a relatively smooth coating.

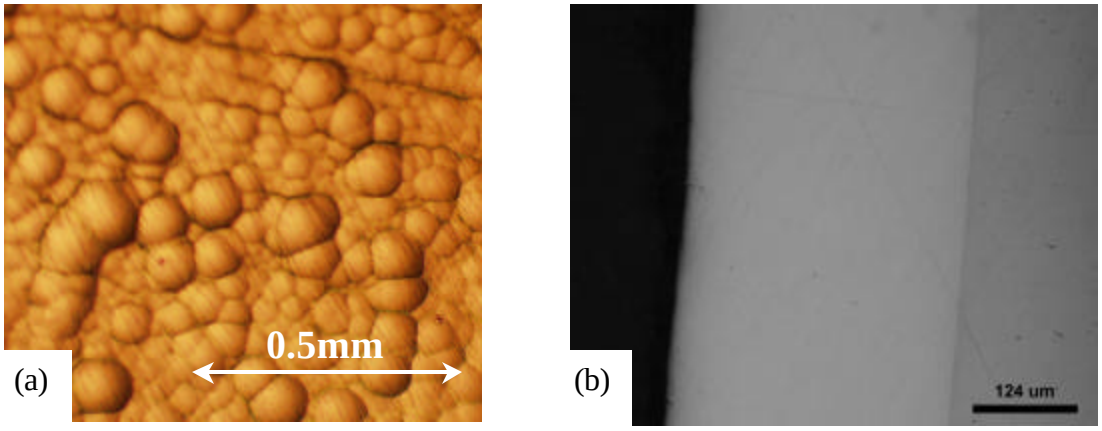

Figure 3-1 Optical micrographs of Nanocrystalline Co 2-3wt%P coatings showing (a) the as-deposited surface at 500x magnification and (b) the cross-section of a 13 mils coating on the ID of a one-inch pipe.

3.2 X-RAY DIFFRACTION ANALYSIS

X-Ray diffraction analysis was performed on the nanocrystalline Co-P coatings as a means of determining the crystal structure and texture as well as estimating the average grain size of the material. The average grain size was determined using Scherer's line broadening formula [13]:

$$d = \frac{0.9l}{b_c \cos q_{hkl}} \tag{3-1}$$

where d is the grain diameter, λ is the x-ray wavelength, β_c is the corrected peak width and θ_{hkl} is the Bragg angle for a given crystallographic plane with Miller indices hkl. The corrected peak width accounts for line broadening that is inherent in the diffractometer and is calculated as follows:

$$b_c = \sqrt{b_{meas}^2 - b_{std}^2} \tag{3-2}$$

where β_{meas} is the total measured width of the peak measured at half the maximum intensity over the background (FWHM) and β_{std} is the broadening for the polycrystalline standard of the same composition.

Figure 3-2 shows typical x-ray diffraction patterns of polycrystalline, nanocrystalline and amorphous Co-P deposits that have been produced in this project. The XRD patterns show that the crystal structure is hexagonal close packed (HCP) which is the equilibrium structure typically found in conventional cobalt at room temperature. Through pulse plating and modifications to the bath chemistry a nanocrystalline structure can be consistently obtained in the composition range from 0 to 6wt% phosphorus. Above 6wt% phosphorus an amorphous structure is typically observed. The average grain size of the optimized Co-P coatings was typically in the range of 5 to 15nm. An average grain size in this range gave the optimum combination of strength and ductility. Decreasing the grain size beyond 5nm results in significantly decreased ductility with no increase in hardness due to a breakdown in the Hall-Petch strengthening mechanism. Increasing the grain size above 15nm results in decrease in hardness.

3.3 ELECTRON MICROSCOPY

Transmission electron microscopy was used to directly observe ultra-fine grain structure of the nanocrystalline Co 2-3wt%P coatings. Figure 3-3 shows a bright field, dark field and diffraction pattern micrographs obtained from the TEM. The micrographs reveal a relatively narrow grain size distribution in the material, with an equiaxed grain structure with most grains ranging in size from 5 to 15nm (reaffirming the XRD results). The diffraction pattern shows the typical "ring" pattern typically observed with ultra-fine grain sized materials, and no diffraction spots were observed that correspond to cobalt-phosphites, indicating that the phosphorus is present in the deposits in a solid solution state (similar to XRD results).

Figure 3-4 shows an SEM micrograph of a typical cross-section through a nanocrystalline composite coating consisting of a nanocrystalline Co 2-3wt% P matrix with boron carbide (B_4C) particulate. The micrograph reveals a uniform distribution of particulate throughout the matrix with little agglomeration of particulate.

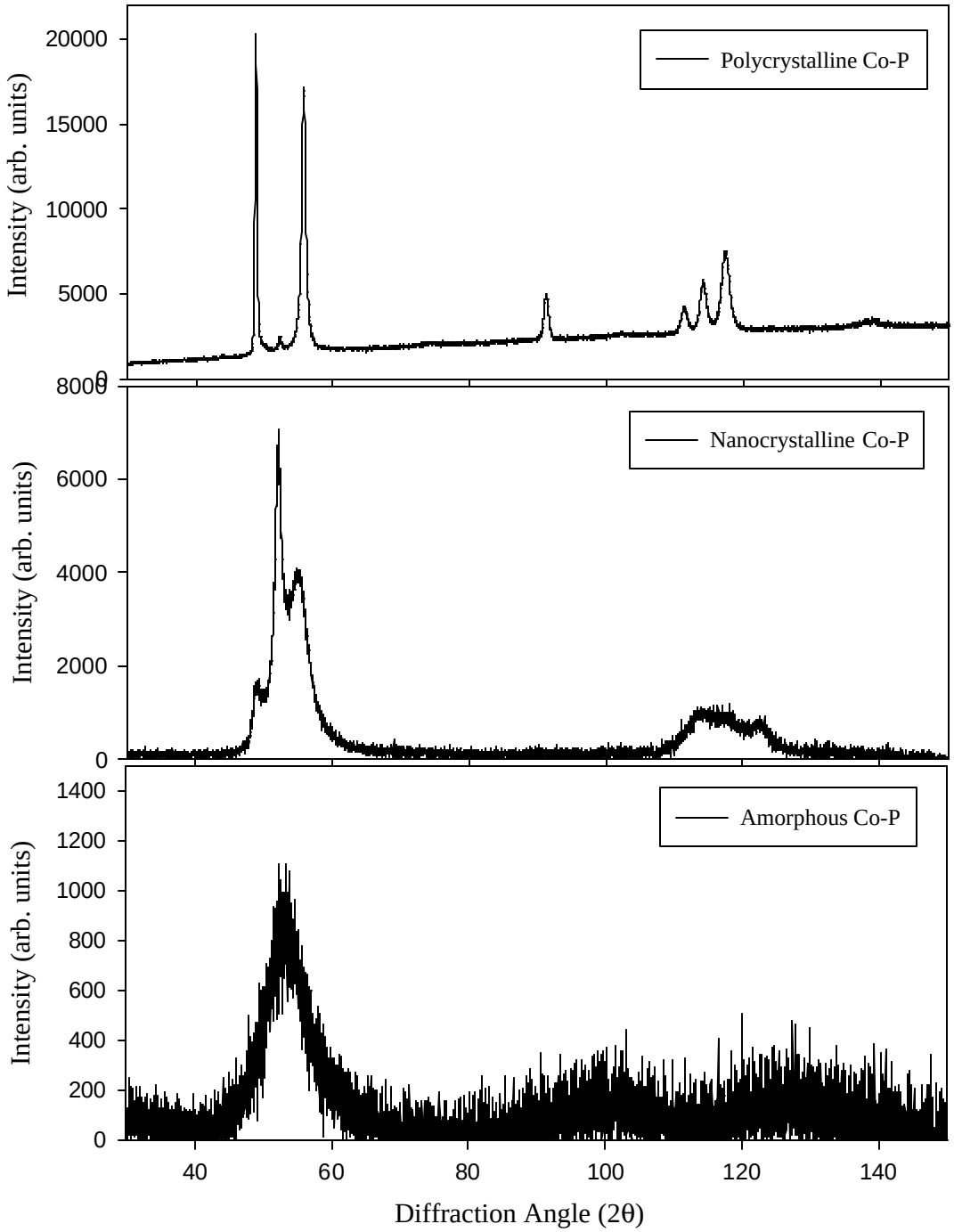

Figure 3-2 X-Ray diffraction patterns for polycrystalline, nanocrystalline and amorphous cobalt phosphorous electrodeposits

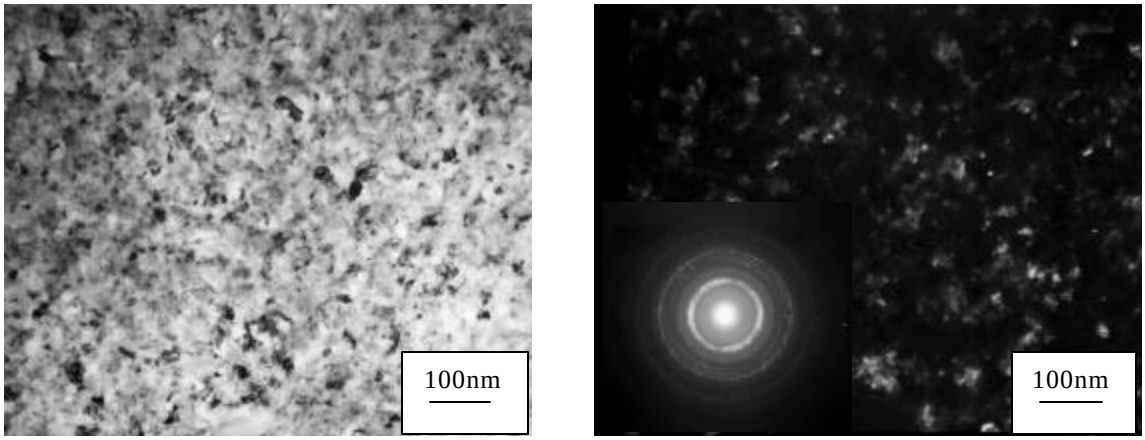

Figure 3-3 a) Bright field, b) dark field and spot diffraction pattern (inset) transmission electron micrographs (TEM) of nanocrystalline Co 2-3wt% P

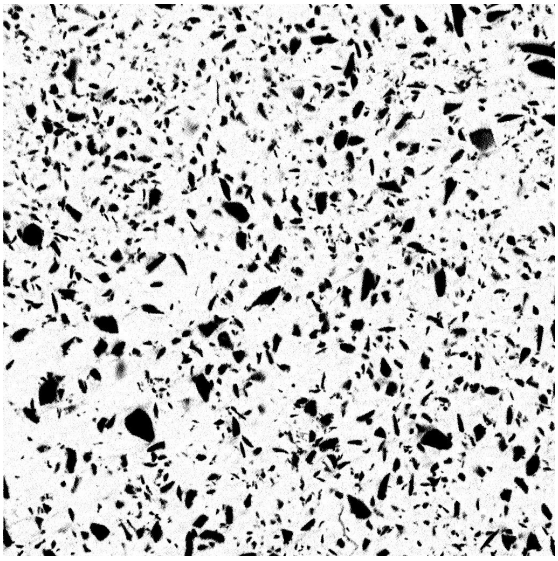

Figure 3-4 SEM micrograph of a typical cross-section through a nanocrystalline Co-P composite coating consisting of a nanocrystalline Co-P matrix with B_4C particles.

4.0 PROPERTIES

4.1 MECHANICAL STRENGTH

4.1.1 Vickers Microhardness

4.1.1.1 As-Deposited

As a result of Hall-Petch strengthening, nanocrystalline Co-P alloys display significant increases in hardness and strength relative to their coarser grained counterparts due to their ultrafine grain size. A further increase in hardness can be achieved through a solid solution hardening mechanism by alloying with phosphorus. The effect of phosphorus content on the hardness of nanocrystalline cobalt electrodeposits is shown in Figure 4-1. The figure shows a linear increase in the as-deposited hardness with increasing phosphorus content. The solid solubility of phosphorus in cobalt is negligible [14], however, a considerable extension of the solid solubility range has been observed in the present study, as Co-P solid solutions were obtained with phosphorus concentrations of more than 5wt%. Similar extended solubility ranges have been previously observed in other nanocrystalline alloys produced by electrodeposition, such as Ni-P [15,16], Co-W [17], Zn-Ni [18] and Ni-Mo [19]. As a result of this extended solubility range, the hardness was observed to increase from approximately 550 VHN, for pure nanocrystalline cobalt (grain size ~14nm), to over 800 VHN for nanocrystalline cobalt containing 5wt% phosphorus.

4.1.1.2 Annealed

A further increase in hardness, via a precipitation hardening mechanism, can be obtained by annealing the as-deposited material to induce the precipitation of cobalt-phosphites from the supersaturated solid solution at elevated temperatures. Figure 4-2 shows the variation in hardness as a function of annealing time at 400°C for up to 30 minutes, for three cobalt-phosphorus deposits with different concentrations of phosphorus and a pure nanocrystalline cobalt deposit. The three cobalt-phosphorus deposits show an increase in hardness with annealing time passing through a maximum after around 10 minutes, followed by a slow decrease with increasing time. It should be emphasized at this point that through a short heat treatment process, presence of phosphorus in the deposit results in an additional increase in hardness to values close to those for the upper limit of hard chrome. A similar trend has also been observed for electrodeposited nanocrystalline nickel-phosphorus alloys [20]. The hardness of pure cobalt deposits, however, only decreases with increasing annealing time. The loss in hardness during the annealing of pure nanocrystalline cobalt is the result of grain growth occurring at this temperature. The general trend indicates that the hardness of nanocrystalline Co-P deposits containing phosphorus concentrations between 3 and 15wt%, can be increased to values exceeding 900VHN by annealing at a temperature greater than 300°C for a suitable period of time.

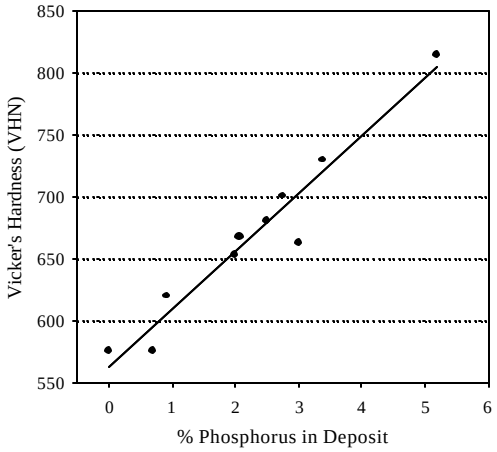

Figure 4-1 Effect of phosphorus concentration on the hardness of nanocrystalline Co-P deposits.

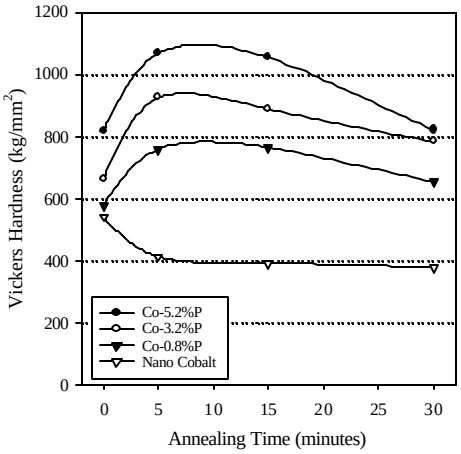

Figure 4-2 Effect of annealing time on the hardness of nanocrystalline Co-P deposits annealed at 400°C.

4.1.1.3 Low Temperature Annealing

The effect of lower temperature annealing (191°C and 250°C) on the hardness of the Co-P deposits was examined. While annealing at 191°C and 250°C did result in an increase in hardness, either the magnitude of the increase was insignificant and/or the time to a significant increase in hardness was unreasonable. Therefore it was concluded that annealing at a temperature lower than 300°C would not result in a significant increase in hardness within a practical time frame.

4.1.2 Tensile Strength and Ductility

In a recent study [21], the tensile properties of electrodeposited nanocrystalline cobalt (produced by the same process) were compared with that of a coarse grained polycrystalline counterpart (see figure 4-3). Significant increases in strength were obtained while maintaining considerable ductility. The greater than two-fold increase in yield and tensile strength while maintaining considerable ductility is quite remarkable and an attractive property when compared to hard chrome coatings, which possess a tensile elongation of less than 0.1%.

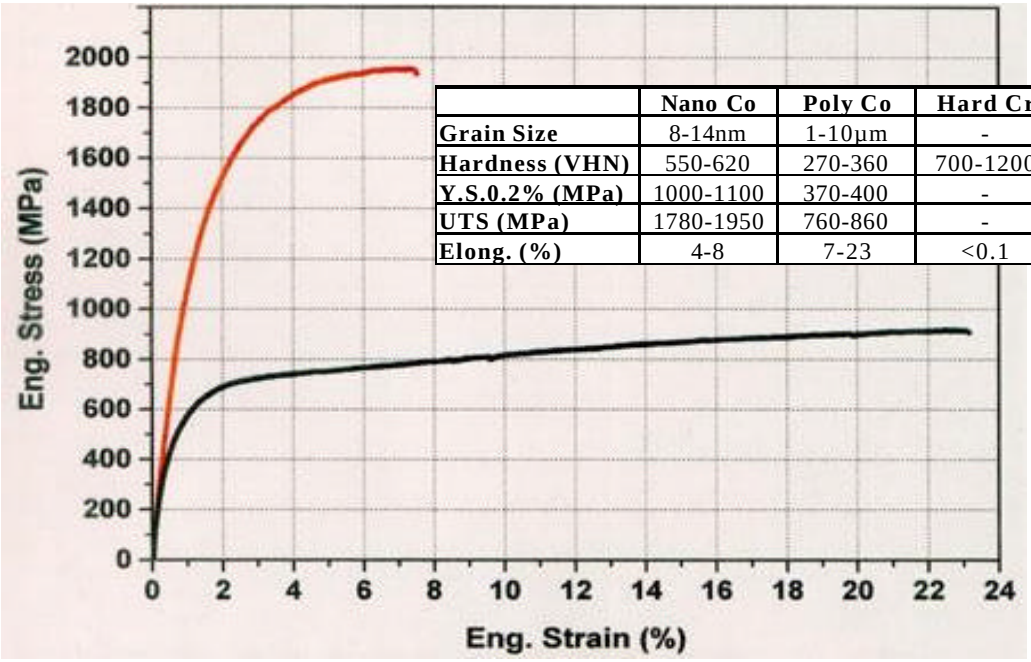

	Nano Co	Poly Co	Hard Cr
Grain Size	8-14nm	1-10µm	-
Hardness (VHN)	550-620	270-360	700-1200
Y.S.0.2% (MPa)	1000-1100	370-400	-
UTS (MPa)	1780-1950	760-860	-
Elong. (%)	4-8	7-23	<0.1

Figure 4-3 Engineering stress-strain curve showing the tensile properties of electrodeposited nanocrystalline cobalt and conventionally prepared polycrystalline cobalt[18].

Due to solid solution strengthening, an increase in the yield and ultimate tensile strengths of nanocrystalline cobalt is expected with the addition of phosphorous. Figure 4-4 shows the results of ASTM B489 ductility bend tests on nanocrystalline Co-P deposits ranging from 0-6wt%P showing the effect of phosphorus on the ductility of nanocrystalline Co-P alloys. The curve shows that the ductility of the coating decreases with increasing phosphorus concentration in the deposit, but that at 5-6wt%P a ductility of 2-3% is still obtained, which is much higher than that of hard chrome coatings.

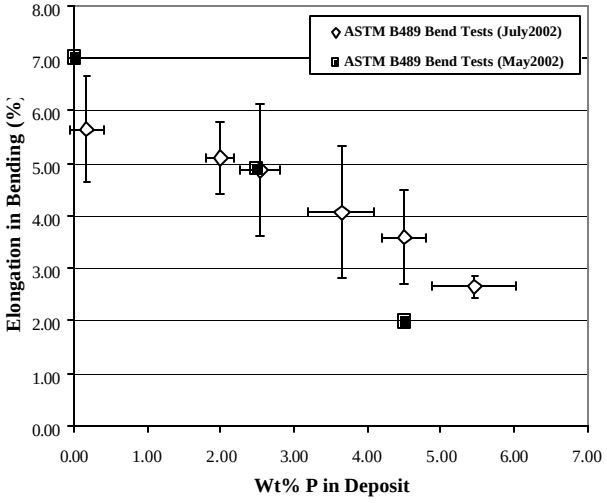

Figure 4-4 Ductility (in bending) of nanocrystalline Co-P deposits as a function of phosphorus concentration.

4.2 THERMAL STABILITY

Due to the ultra-fine grain size in nanocrystalline materials, there is a large driving force for grain growth due to the stored energy at the grain boundaries. As a result, nanocrystalline materials have definitive thermal stability limit, as seen by the loss in hardness in the pure cobalt deposit after an annealing treatment at 400°C for 30 minutes (figure 4-2).

Figure 4-5 shows the XRD patterns for nanocrystalline cobalt in the as-deposited state and after an anneal treatment at 400°C for 30 minutes. From these patterns it is seen that there is a significant change in the structure of the deposit and that the grain size increases from ~13nm to greater than 100nm after annealing. Figure 4-6 shows the XRD patterns for a nanocrystalline Co~3.2wt%P deposit in the as-deposited state and after annealing at 400°C for 30 minutes. From these patterns it is seen that the presence of 3.2wt%phosphorus in the deposit significantly increases the thermal stability of the structure, as the grain size of the as-deposited material only increased from approximately 9nm to 13 nm after annealing, as compared to an increase from 13nm in the as-deposited state to greater than 100nm after annealing for pure cobalt. The thermal stabilization of the structure may be due in part to (a) a solute drag mechanism, or (b) a Zener-type dragging mechanism [22] whereby a force that opposes the driving force for grain growth acts on the grain boundaries due to the formation of small cobalt-phosphide precipitates. Therefore, the presence of phosphorus in the deposit not only results in an increase in the as-deposited hardness of the sample, it also increases the thermal stability of the structure.

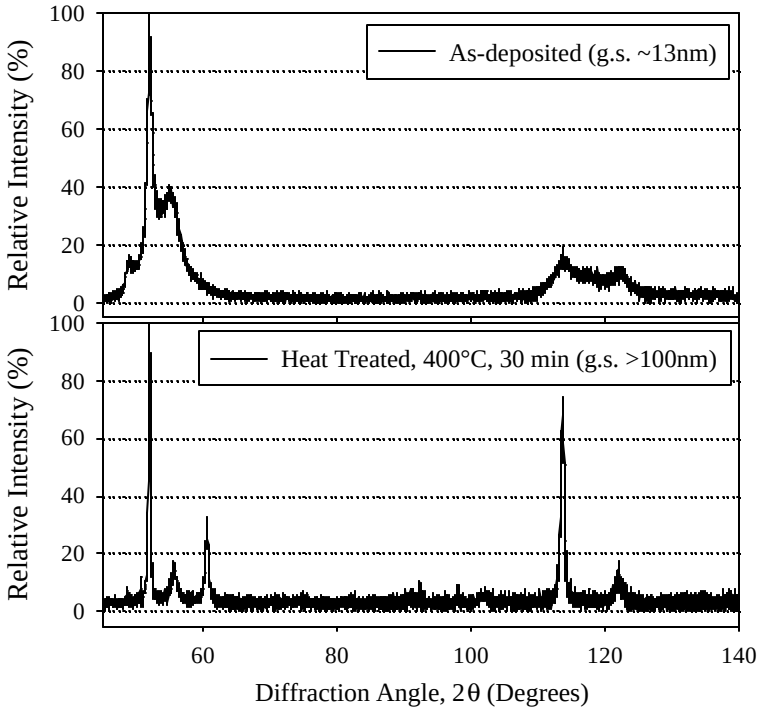

Figure 4-5 X-Ray diffraction patterns of as-deposited and heat treated (400°C, 30 minutes) nanocrystalline cobalt.

Another consequence of their ultra-fine grain size is an increased electrical resistivity over polycrystalline materials due to their high volume fraction of grain boundaries. By measuring the electrical resistivity at elevated temperatures, the temperature at which the material is no longer thermally stable can be determined by a sharp decrease in the electrical resistivity arising from the onset of grain growth. Figure 4-7 shows the electrical resistivity as a function of temperature from 25°C to 700°C for two nanocrystalline cobalt-phosphorus samples and a pure nanocrystalline cobalt sample. The figure shows that the onset of grain growth (as indicated by the large drop in resistivity) increases from 350°C for pure nanocrystalline cobalt to 475°C and 485°C for nanocrystalline Co-0.56%P and Co-3.10%P, respectively. Therefore, the presence of phosphorus in the deposit creates a stabilizing effect on the nanocrystalline grain structure.

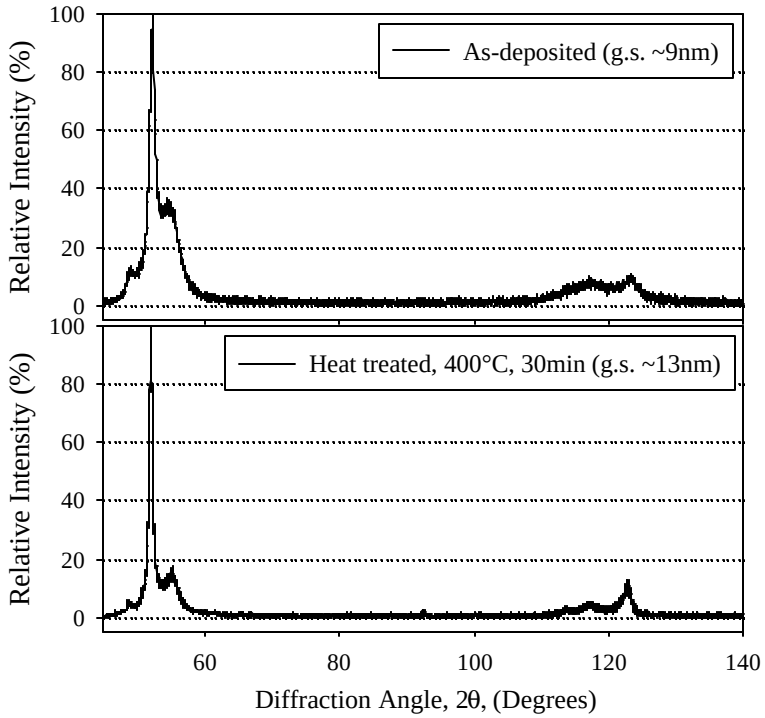

Figure 4-6 X-Ray diffraction patterns of as-deposited and heat treated (400°C, 30 minutes) nanocrystalline cobalt-3.2% phosphorus.

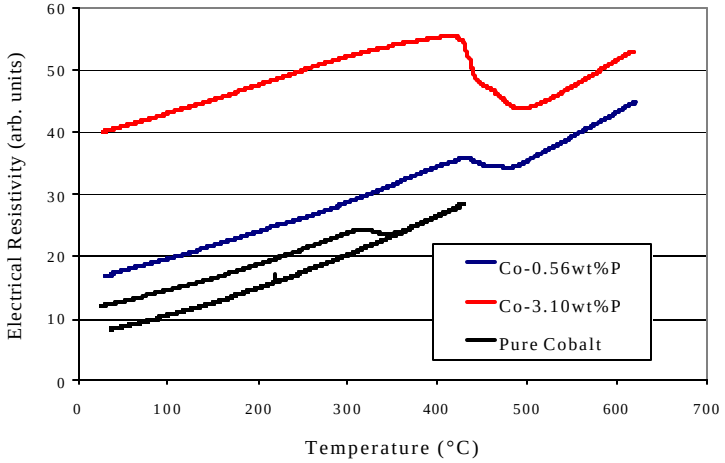

Figure 4-7 Electrical Resistivity as a function of temperature for three nanocrystalline Co-P Alloys.

4.3 WEAR RESISTANCE

4.3.1 Abrasive (Taber) Wear (CS-17 abrasive wheels)

Taber wear measurements were performed on various nanocrystalline alloys produced in this program to determine the abrasive wear properties of the coatings. The following is an excerpt from a recent publication[23] explaining the Taber wear measurement:

> "Taber wear testing is an industry-accepted standard method to evaluate the abrasive wear properties of many materials. Two abrasive wheels are placed on the specimen with a specific load, and a sliding wear action occurs in the contact area when the specimen is rotated, making the unique 'X' wear patterns by the two wheels. For this project, CS-17 abrasive wheels composed of rubber with embedded aluminium oxide abrasive particles (particle size: 50~200μm) were used. Table 1 shows the test conditions of the Taber wear test based on ASTM D 4060, ASTM C 501, U.S. military specification MIL-A-8625F and Japanese Industrial Standard H 8503. After every 1,000 cycles, the specimen was ultrasonically cleaned in acetone for 5 minutes before the weight loss was measured using a 0.1mg resolution scale. The surfaces of the abrasive wheels were refaced using 150 grit size SiC paper to avoid clogging or contamination by worn particles. Three samples were tested for each nanocrystalline alloy."

The composition, crystal structure, grain size, Vicker's hardness and Taber Wear Index for various nanocrystalline cobalt, cobalt-phosphorus, cobalt-iron and cobalt-iron-phosphorus samples are shown in Table 4-1.

A relationship commonly used to describe the improvement of the wear resistance with hardness is known as Archard's law:

$$\Delta V = k\frac{L \cdot S}{H} \qquad (4\text{-}1)$$

where: DV is the volume loss, k is the wear coefficient, L is the applied load, S is the sliding distance and H is the hardness of the material.

The relationship between inverse hardness and TWI for the various cobalt, cobalt-phosphorus, cobalt-iron and cobalt-iron-phosphorus deposits is shown in Figure 4-8. At first glance, the data seems rather scattered, but when separated into divisions based on the concentration of iron in the deposit, the TWI generally decreases with increasing hardness, more or less in accordance with Archard's Law.

The various nanocrystalline cobalt-iron alloys indicate that the TWI decreases with increasing iron concentration, decreasing from 38.7 for a cobalt deposit with 0wt%Fe to 6.8 for a deposit with 88.5wt% Fe. If Archard's law is assumed to be valid for a given composition then the wear coefficient, k (equation 4-1), can be estimated based on the TWI and the hardness. Figure 4-9 shows the variation of the wear

coefficient for cobalt-iron alloys as a function of iron content, showing a decreasing wear coefficient with increasing iron content. Some factors that may contribute to the variation of the wear coefficient with iron content are the crystal structure, ductility, surface energy, grain size, etc.

Based on the estimated wear coefficients for the Co-Fe alloy system presented in Figure 4-9, the TWI can be predicted for various Co-Fe alloys as a function of hardness. Figure 4-8 shows the predicted variation of the TWI for various concentrations of iron for the cobalt-iron alloy system as a function of inverse hardness as dotted lines along with the experimental data. From this curve it is possible to roughly estimate the TWI for a given cobalt-iron alloy of specific hardness.

Table 4-1 Composition, crystal structure, grain size, hardness and Taber wear index of all the samples tested to date.

Sample	***Composition***	***Crystal Structure***	***Grain Size***	***Vickers Hardness (VHN)***	***Taber Wear Index (mg/1000cycles)***
STANDARDS					
Mild Steel	-	BCC	N/A	150	31.7
Tool Steel	-	BCC	N/A	258	21.4
Stellite	70%Co, 21%Cr, 4.5%W, 3.5%Ni, 1%Fe	FCC	N/A	453	7.4
HVOF	82%W, 10%Co, 4%Cr, 3.5%C	N/A	N/A	1390	3.6
Hard Chrome	100% Cr	BCC	N/A	1208	3.4
NANOCRYSTALLINE					
Cobalt	100% Co	HCP	15 nm	500	38.2
Cobalt	100% Co	HCP	12 nm	554	38.7
Co 1-2wt%P	99%Co, 1%P	HCP	<10 nm	680	29.4
Co 4-5wt%P	95%Co, 5%P	HCP	<10 nm	745	27.7
Co 4-5wt%P (HT 8min, 450°C)	95%Co, 5%P	HCP	<10 nm	1013	27.3
Co 15-20wt% P	82%Co, 18%P	-	Amorphous	657	24.7
Co 15-20wt% P (HT 1hr, 350°C)	82%Co, 18%P	HCP	<10 nm	904	12.1
Co 2-3wt% P w/ 30vol% B_4C	2-3wt%P 30 vol% B_4C	HCP	<10 nm	585	2.3
Co-Low Fe	97%Co, 3%Fe	Mixed HCP/FCC	<15nm	510	38.2
Co-High Fe	68%Co, 32%Fe	BCC	>30nm	340	29.8
Co-Low Fe-P	80%Co, 19%Fe, 1%P	BCC	<20nm	467	27.7
Co-High Fe-P	68%Co, 29%Fe, 3%P	BCC	<15nm	884	11
Fe-Low Co-P	88.5%Fe, 9.5%Co, 2%P	BCC	<20nm	706	6.8
Iron	99.5%Fe, 0.5%Mn	BCC	~20 nm	871	4.3

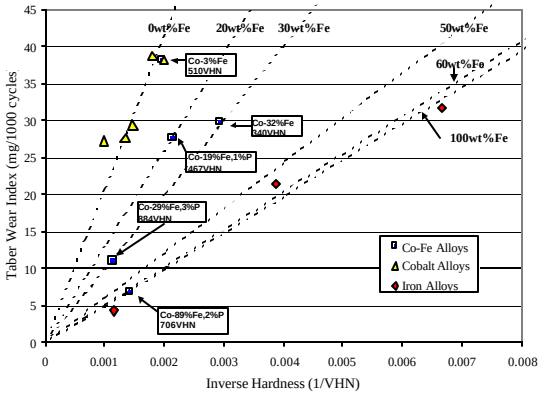

Figure 4-8 Estimated correlation of TWI with hardness for cobalt-iron alloys of various iron concentrations. The symbols represent actual experimental data.

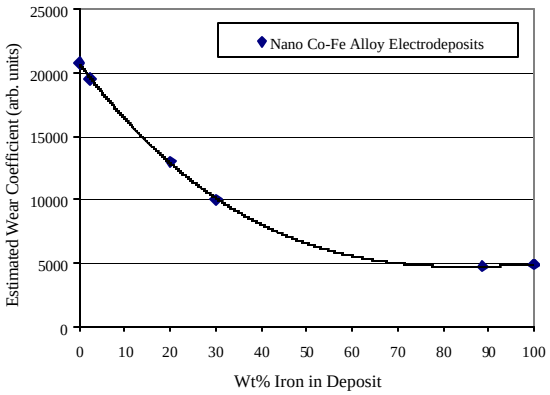

Figure 4-9 The variation of the wear coefficient, *k*, with iron content for cobalt-iron alloy electrodeposits.

The Taber wear index of CoP-B_4C composite deposits was measured as a function of the volume fraction of B_4C in the deposit. Table 4-2 gives the results of these tests. Figure 4-10 shows that the TWI significantly decreases with increasing B_4C content in the deposit. When the volume fraction of B_4C in the deposit increased above approximately 15vol%, the TWI is found to decrease to values below that of chrome (~3.4 mg/100cycles).

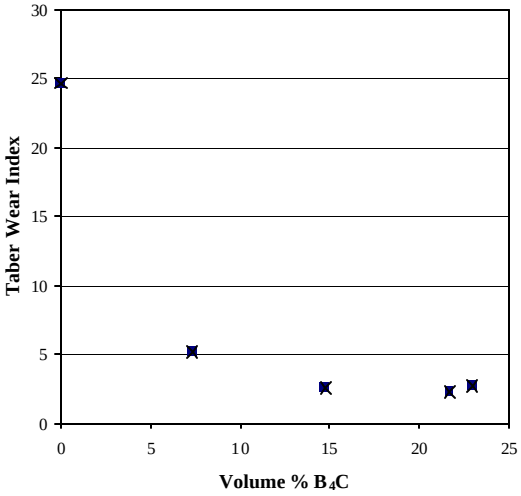

Figure 4-10 Taber wear index of nanocrystalline Co-P B_4C composite coatings as a function of B_4C content in the deposit.

Table 4-2 Vickers hardness and Taber wear index of electrodeposited Co~18wt%P in the as-deposited and heated condition.

Sample		Vickers Hardness (VHN)	Taber Wear Index (mg/1000cycles)
Nano Co2-3wt%P w / B_4C	0 vol% B_4C	~600	28.3
	7 vol% B_4C		5.2
	15 vol% B_4C		2.5
	22 vol% B_4C		2.3
	23 vol% B_4C		2.7

4.3.2 Abrasive (Taber) Wear (CS-10 abrasive wheels)

Two nanocrystalline cobalt and two nanocrystalline Co-P samples were re-tested in the Taber Wear (abrasive) tester using the less abrasive CS-10 wheels (commonly used in industry). The previous nanocrystalline Co and Co-P alloys were tested using the highly abrasive CS-17 wheels. Table 4-3 shows the results of the Taber test using these wheels along with the composition, structure and hardness data on the alloys tested. These tests indicated that a 46 to 60% drop in the TWI occurs when using the CS-10 wheels in place of the CS-17 wheels. Figure 4-11 shows X-Ray diffraction (XRD) patterns for the four Co-alloy Taber test samples. Three of the samples show typical crystallographic textures commonly observed throughout the program (Figures 4-11b-d). One sample, however (Figures 4-11a) shows a significant deviations from this texture. It is interesting to note that out of the two pure Co samples, the one that is textured such that the Basal plane is not parallel to the surface has the lower Taber wear index even though is 170 VHN softer. This indicates the significant effect that crystallographic texture has on the wear behaviour of the nanocrystalline Co-P alloys coatings.

Table 4-3 Composition, structure, hardness and Taber Wear results for various Co and Co-P electrodeposits.

Composition	*Grain Size*	*Hardness (VHN)*	*TWI (CS-10)*	*Estimated TWI using CS-17*	*% Change*
Pure Co	22 nm	297	16.6	N/A	N/A
Pure Co	12 nm	470	20.4	38	-46%
Co-1.2wt%P	6 nm	545	14.5	31	-53%
Co-3.5wt%P	15 nm	575	11.0	28	-60%

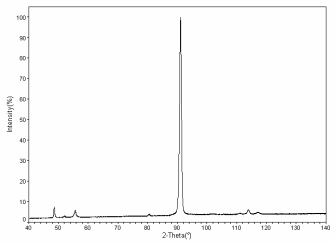

(a) Nano Co (22nm)

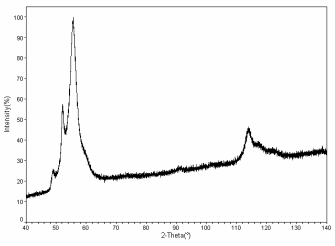

(b) Nano Co (12nm)

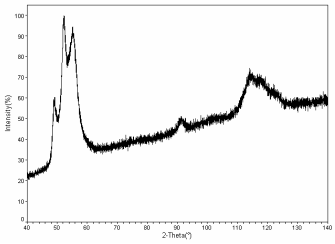

(c) Nano Co-1.2wt%P (6nm)

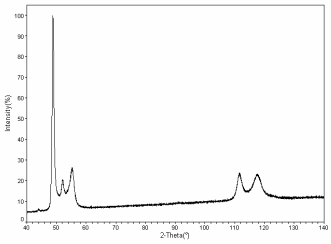

(d) Nano Co-3.5wt%P – (12nm)

Figure 4-11 X-Ray diffraction patterns of nanocrystalline Co and Co-P abrasive (Taber) wear test samples using CS-10 abrasive wheels.

4.3.3 Sliding (Pin-On-Disk)

Sliding wear (Pin-on-disk) measurements were performed (using a CSEM Tribometer) on various nanocrystalline Co-P alloys as well as various standard materials including: mild steel, tool steel and hard chrome. Measurements were performed according to the ASTM G99 standard. All samples were polished to a 1-micron finish and were ultrasonically cleaned in isopropanol prior to tested. Wear measurements were made using a load of 10N, a sliding velocity of 0.1 m/s, a total sliding distance of 1000m and a 6mm alumina (Al_2O_3) ball as the static friction member. On each sample wear measurements were performed using a 10mm diameter wear track. Measurements were made in un-lubricated dry laboratory air. A stylus profilometer was used to measure the cross-sectional area of the wear track to yield the volume loss of the plate.

Table 4-4 shows the hardness and sliding wear data for the various materials tested and Figure 4-12 shows examples of typical wear profiles for nanocrystalline Co, Co 4wt%P, Co 18wt%P, CoP-B_4C composite and hard chrome. In general, the sliding wear volume losses for the nanocrystalline alloys were found to be lower than the reference materials, including mild steel, tool steel and hard chrome. A significant drop in wear rate was observed with the addition of 2wt% phosphorus to pure cobalt sample, but little improvement was seen after 2wt%, even though the composition of phosphorus in the test samples varied from 2 and 10wt%. A nanocrystalline Co~4wt%P was tested after hardening by a heat treatment at 400°C for 10minutes, and although the hardness increased by 35%, no significant improvement in the wear resistance was observed. A Co 18wt%P deposit heat-treated at 350°C for 1 hour with a hardness of 904VHN was found to have an extremely low wear rate (0.4×10^{-6} mm^3/Nm).

Table 4-4 Hardness and sliding wear data for various standard and nanocrystalline materials.

Material	***Hardness (VHN)***	***Coefficient of Friction***	***Wear Volume Loss (mm^3/Nm) x 10^{-6}***
Standard Samples			
Mild Steel	150	0.73	18.2
Tool Steel	250	0.75	13.1
Hard Chrome	1200	0.70	11.9
Nanocrystalline Samples			
Nano Cobalt	500	0.35	10.7
Nano Co~2%P	730	0.53	5.5
Nano Co~4%P	745	0.48	6.4
Nano Co~4%P (HT)	1010	0.44	5.3
Nano Co~6%P	730	0.45	7.1
Nano Co~10%P	720	0.50	6.2
Co~18%P (HT)	904	0.63	0.4

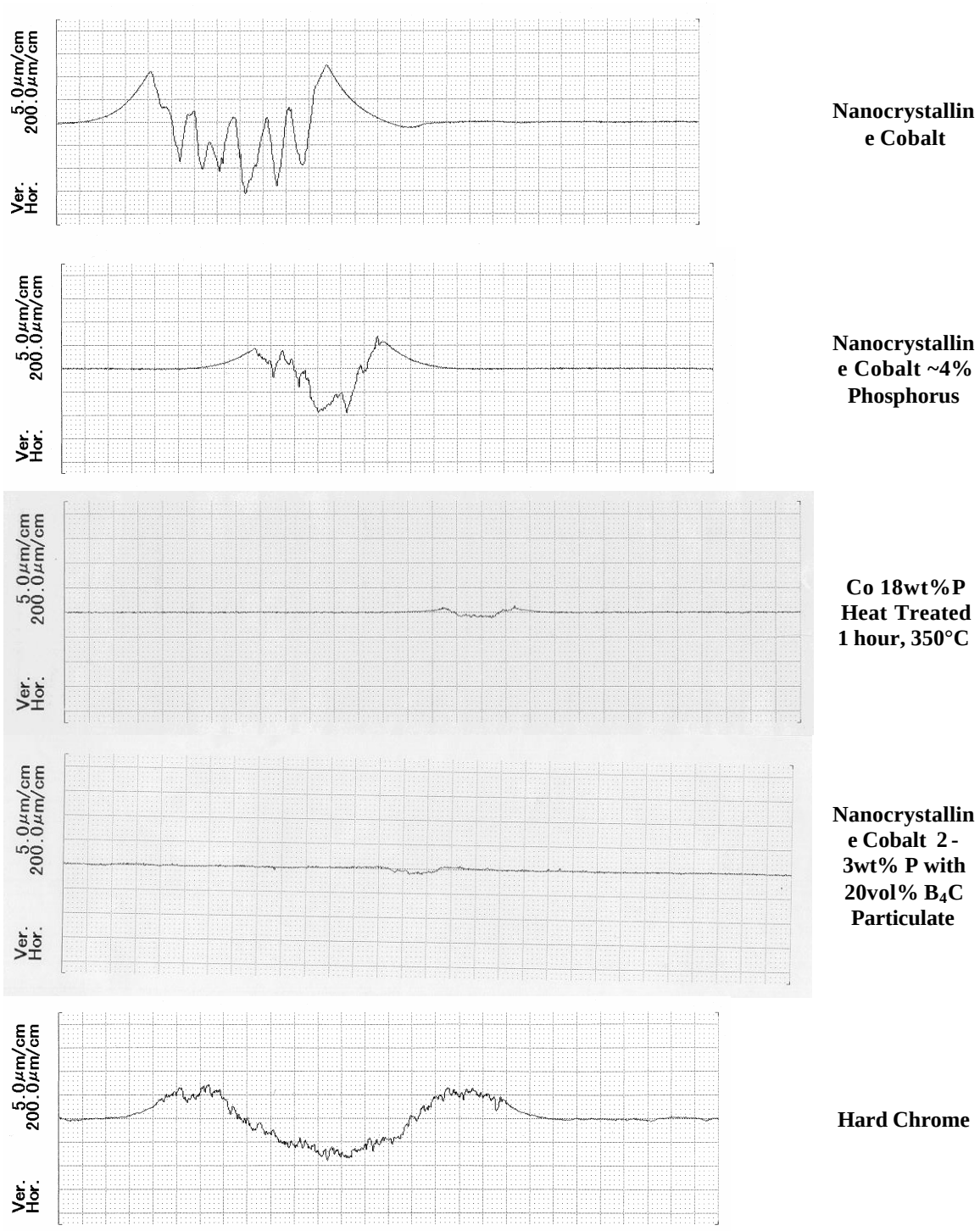

Figure 4-12 The wear track profiles for nanocrystalline cobalt, heat treated nanocrystalline Co~5wt%P, nanocrystalline Co 2-3wt%P with 20vol% B_4C and hard chrome control sample tested under sliding wear conditions using a 10N load, 1000m total sliding distance, 10mm wear track diameter and sliding velocity of 10cm/s.

To assess the relationship between sliding wear behaviour and phosphorus content (in the as-deposited and annealed state), sliding wear (Pin-on-disk) measurements were performed on three nanocrystalline Co-P alloys with 2wt%, 6wt% and 10wt%P, respectively, in the as-deposited state and after annealing at 191°C for 500 hours. Measurements were performed according to the ASTM G99 standard as described above.

Table 4-5 shows the results of sliding wear tests on nanocrystalline Co-P deposits with 2, 6 and 10wt% Phosphorus, in the as-deposited and heat-treated state (500hrs at 191°C). The results show that the wear volume loss is similar to what has been previously reported for nanocrystalline Co-P alloys. There was no clear correlation between the level of phosphorus and the wear resistance of the material. The effect of the low temperature annealing treatment was also found to have no significant effect on the wear resistance.

Table 4-5 Hardness and sliding (pin-on-disk) wear data for various nanocrystalline Co-P alloys in the as-deposited state.

	As-Deposited			**Annealed – 191°C, 500 hours**		
Sample	Hardness (VHN)	Coefficient of Friction (μ)	Wear Volume Loss (mm^3/Nm)*	Hardness (VHN)	Coefficient of Friction (μ)	Wear Volume Loss (mm^3/Nm)*
Co-2wt%P	728	0.53±0.13	5.5×10^{-6}	765	0.44±0.09	6.98×10^{-6}
Co-6wt%P	733	0.45±0.08	7.09×10^{-6}	830	0.88±0.11	5.1×10^{-6}
Co-10wt%P	719	0.50±0.01	6.17×10^{-6}	730	0.45±0.03	6.15×10^{-6}

*estimated wear loss for a 10mm wear track diameter based on values obtained from a 5mm wear track diameter.

4.3.4 Sliding (Pin-on-disk) wear testing with various "Pin" Materials

Sliding wear (Pin-on-disk) measurements were performed on nanocrystalline Co~3wt%P alloy and a hard chrome standard using various materials as the static (Pin) friction member. Wear measurements were made as per the instructions described above with the exception that 6mm mild steel, alumina and tungsten carbide balls were used as the static friction member.

Table 4-6 shows the results of sliding wear tests performed on hard chrome and nanocrystalline Co-P electrodeposits. Each material was tested with a 6mm alumina oxide, tungsten carbide and mild steel ball as the static friction member. The results

show that the wear volume loss for nanocrystalline Co-P was lower than that for electrodeposited hard chrome when hard ceramic material is used as the static friction member (5.5 to $6.4x10^{-6}mm^3/Nm$ compared to $11.0\text{-}11.9x10^{-6}mm^3/Nm$). When a mild steel ball was used, however, no wear was observed on the Hard chrome, but severe wear was observed on the mild steel ball. The wear volume loss for the nanocrystalline Co-P, however, was similar (varied between 5.5 and 6.4 x $10^{-6}mm^3/Nm$), regardless of the material of the ball.

Table 4-6 Pin-on-disk (sliding/adhesive) wear results for Hard Chrome and Nanocrystalline Co-P when worn against various static ball materials.

Disk / Pin Material	Coefficient of Friction (μ)	Plate Volume Wear (mm^3/Nm)	Ball Wear
Hard Chrome / Al_2O_3	0.699	11.9×10^{-6}	Low
Hard Chrome / WC	0.693	11.0×10^{-6}	Mild
Hard Chrome / Mild Steel	0.871	Negligible	Severe
Nano Co-P / Al_2O_3	0.480	6.4×10^{-6}	Low
Nano Co-P / WC	0.518	5.5×10^{-6}	Low
Nano Co-P / Mild Steel	0.695	6.1×10^{-6}	Low

4.4 CORROSION RESISTANCE

4.4.1 Salt Spray

Nanocrystalline Cobalt-phosphorus and cobalt-iron-phosphorous deposits (0.002" and 0.010" thick) were electroplated onto Q-Panels and exposed to the environment of a salt spray cabinet operated according to the requirements of ASTM B117-97, "Standard Practice for Operating Salt Spray (fog) Apparatus". Inspections were conducted regularly and photographs of the Q-Panels were taken when removed. Each set was exposed for a period of six weeks. The panels were edge masked using duct tape and placed in the salt spray cabinet oriented longitudinally with the plated surface inclined 15° from the vertical.

The backs of the Q-Panels were masked with electroplater's tape and the edges were masked with wax. The Q-Panels were photographed in groups and exposed in the salt spray environment for 48 hours. The panels were rated by comparing them with Figure X2.2 of ASTM B537 and photographed. The exposure continued for six weeks with weekly evaluations. When the rating of a panel fell to worse than 1, it was removed and photographed. After six weeks exposure, the panels were rated as usual and photographed.

A bare Q-Panel was analyzed using GDS-OES with the following results:

Cr [%]	Mn [%]	Mo [%]	Ni [%]	P [%]	S [%]	Si [%]	C [%]
0.02	0.37	<0.01	0.01	0.005	0.0010	0.03	0.11

The Protection Rating refers to crater rusting, pinhole rusting, rust stain, blisters and any other defects that involve basis metal corrosion. The numerical value obtained by comparison with the charts is related to the area of the panel affected. The Appearance Rating is arrived at by deducting points from the Protection Rating based on the observer's impression of the extent to which the corrosion of the coating detracts from the appearance of the panel.

Figure 4-13 shows the ratings as a function of exposure time of the various nanocrystalline materials as well as standard materials after being exposed to a salt spray environment for up to 1000 hours (as per ASTM B117). Figures 4-14 shows the photomacrographs of the Co-P alloy test panels in the as-deposited condition and after 48hrs and 6week exposure time. The Co 2-3wt% P test samples performed very well, decreasing to only a 9/8 Protection/Appearance rating after 6 weeks exposure time. The thickness of the Co-P coatings was not found to significantly improve the corrosion protection. All of the nanocrystalline Co-Fe-P test samples, however, did not perform well, most showing severe deterioration after the first 48 hours. Co-Fe-P test samples with a nickel strike did seem to slightly improve the protection/appearance rating, but overall did not provide any corrosion protection, suggesting the coating itself may be the source of the red rust.

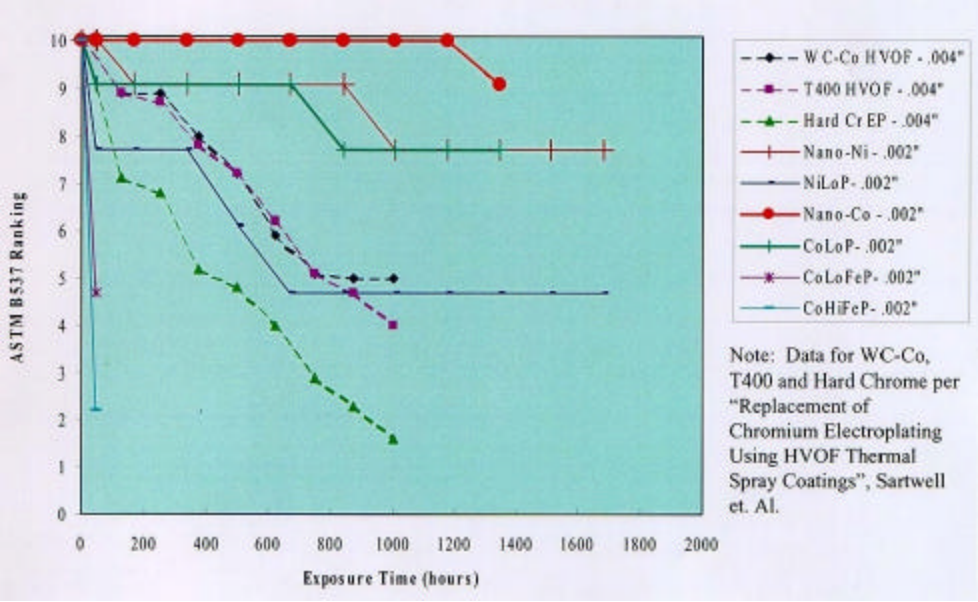

Figure 4-13 ASTM B537 Ranking as a function of exposure time for various nanocrystalline Co-P, Co-Fe-P and Ni alloy coatings along with Hard Cr and HVOF coatings.

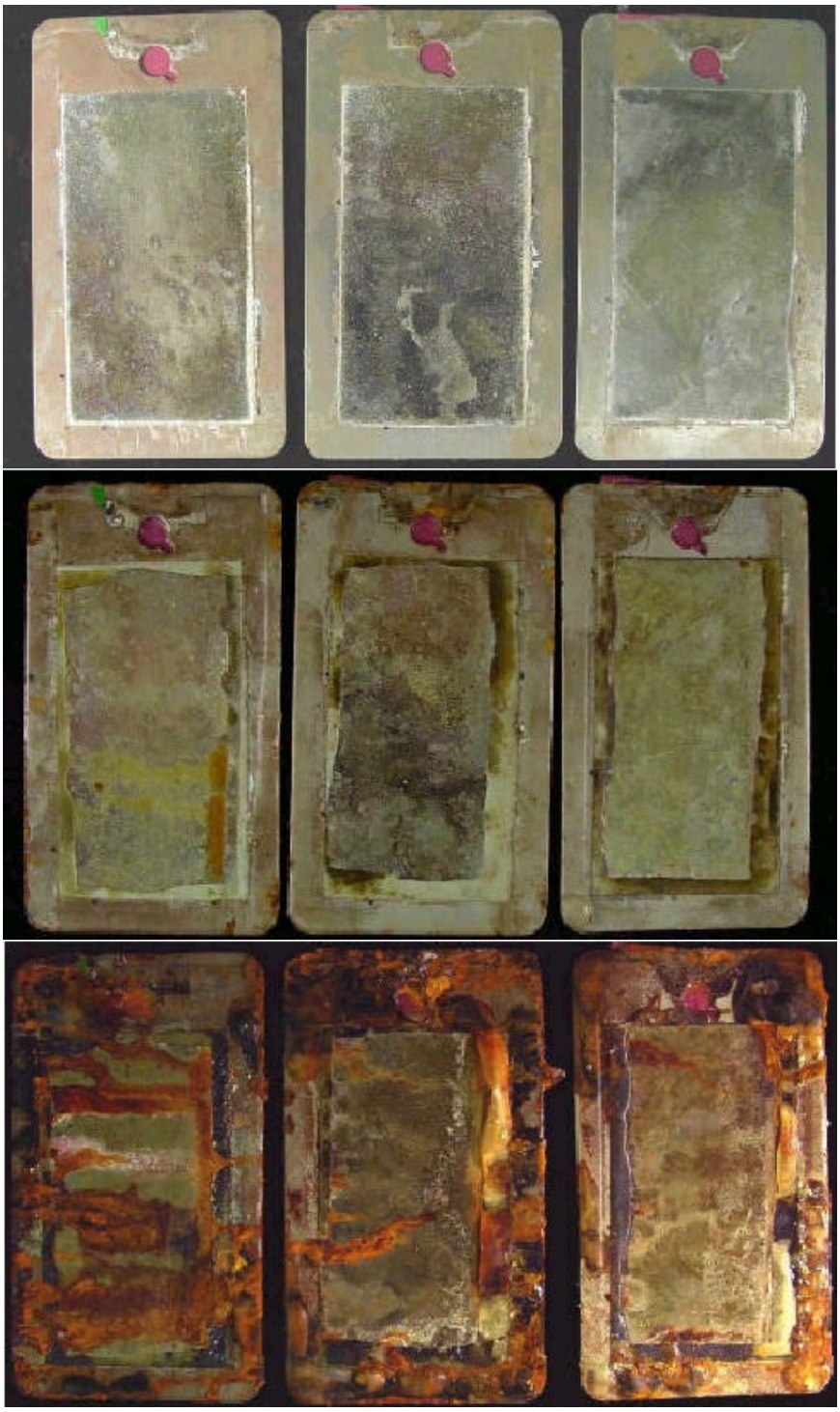

Figure 4-14 Photomacrographs of as-deposited nanocrystalline cobalt 2-3wt% test samples after 0 hours, 48 hours and 6 week exposure in a salt (fog) spray environment per ASTM Standard B117.

4.4.2 Potentiodynamic

Electrochemical potentiodynamic corrosion testing (per ATSM G61) was performed on three (3) standard materials: metallurgical prepared polycrystalline cobalt, nickel 200 and electrolytic hard chrome, as well as on three electrodeposited nanocrystalline alloys: cobalt, cobalt 2-3wt% phosphorus and cobalt 4-5wt% phosphorus. Linear polarization resistance scans (LPR) were performed in 3.56wt% NaCl solution at room temperature. From these measurements the corrosion rate was determined.

Figure 4-15 shows the preliminary results from the experiment showing the corrosion rate for the various materials tested as a function of test time. Generally the corrosion rate was relatively stable with testing time.

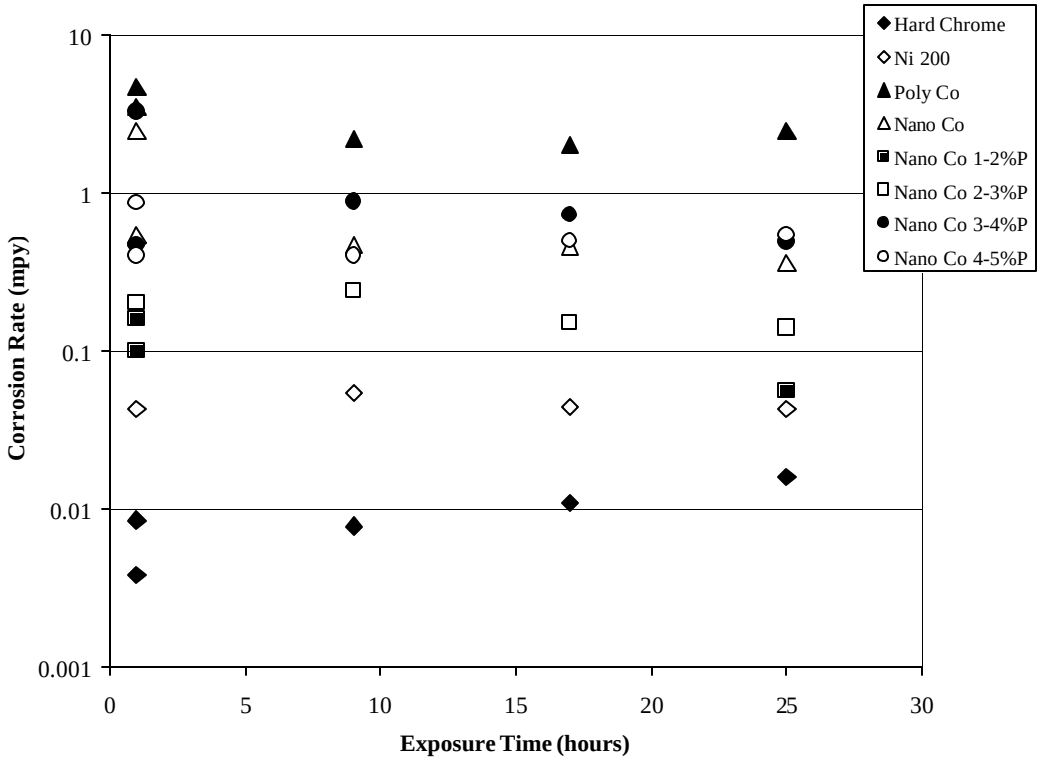

Figure 4-15 Electrochemical corrosion rate of various nanocrystalline Co-P alloys, polycrystalline Co, Ni200 and hard chrome as a function of testing time.

Figure 4-16 shows the preliminary results from the experiment showing the corrosion rates after 25 hours of exposure of nanocrystalline Co-P alloys as a function of phosphorus concentration along with the corrosion rates of Hard Chrome, Ni200 and metallurgically prepared polycrystalline cobalt. As expected, hard chrome had the lowest corrosion rate of all the materials tested due to the formation of its stable oxide film (Cr_2O_3). Polycrystalline cobalt had the highest corrosion rate of all the materials tested, at approximately 2 millimetres per year (mpy). The corrosion rate of nanocrystalline Co-P alloys was found to initially decrease with increasing phosphorus concentration, to approximately 1-2wt%P, and was then found to increase with increasing phosphorus concentration. At 1-2wt%P, the corrosion rate was only slightly higher than that of Nickel 200. From these results a few conclusions can be made: (i) a decrease in grain size improves the corrosion resistance of the material (seen from the improvement in corrosion rate of nanocrystalline cobalt over polycrystalline cobalt), (ii) the addition of small amounts of phosphorus (1-2wt%) to nanocrystalline cobalt results in a further decrease in corrosion rate, and (iii) the corrosion rate of nanocrystalline Co 1-2wt%P is similar to that of Nickel 200.

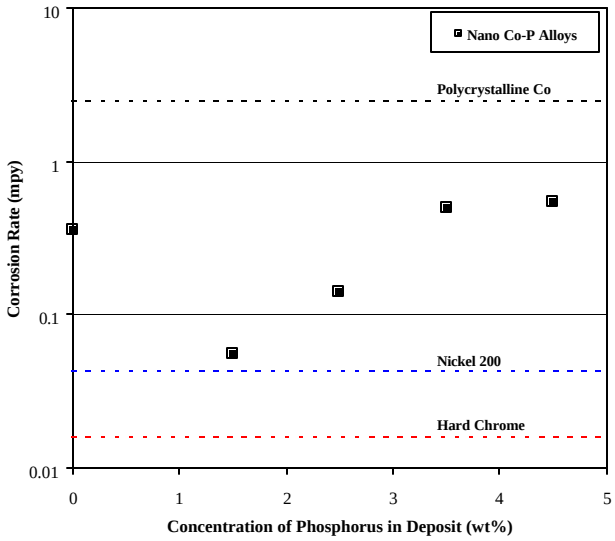

Figure 4-16 Corrosion Rate of various materials as a function of exposure time.

4.5 INTERNAL STRESS

Internal stress measurements were made on the cobalt phosphorus electrodeposits from the standard chloride-based chemistry using a "Deposit Stress Analyzer – Model 683" obtained from Larry King Corp. The effects of bath composition, electrical parameters, temperature and pH on the internal stress of nanocrystalline Co-P coatings were investigated using the standard chloride-based chemistry.

The following excerpt describes the difference between tensile and compressive internal stress in electrodeposits:

> *"A simple analogy can be used to demonstrate the difference between tensile and compressive stress - the two practically important types of*

internal stress in electrodeposits. Deposits having tensile internal stress can be thought of unidimensionally as a stretched coil spring or rubber band (see Fig. 4-17a), attached to a stress-free (before deposition) substrate. Compressively stressed unidimensional deposits, then, will resemble a compressed spring (Fig. 4-17b) attached to the substrate.[24]"

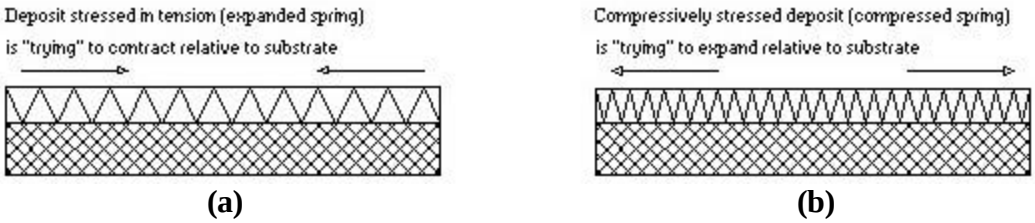

Figure 4-17 Internal stresses seen in electrodeposits: (a) Tensile, (b) compressive.

The internal stress of Co-P deposits was measured on samples deposited using various current densities, pulse conditions, temperatures, pH, cobalt chloride concentrations and phosphorous acid concentrations. While the internal stress of the Co-P deposit was affected by changes in the above-mentioned conditions, it was due to changes in the composition of the deposit caused by a change in conditions. Figure 4-18 shows the internal stress of Co-P deposits as a function of phosphorus concentration in the deposit. The internal stress of the deposits was found to go from highly tensile at low phosphorus concentrations to compressive at high phosphorus concentration.

At a given composition, however, the internal stress of the deposits was found to mildly depend on current density. For Co 2-3wt%P deposits, the internal stress was found to range between 12.5 and 15.5 ksi (85 and 105 MPa) in tension, and was found to increase with increasing current density. This is generally considered to be moderate-to-high.

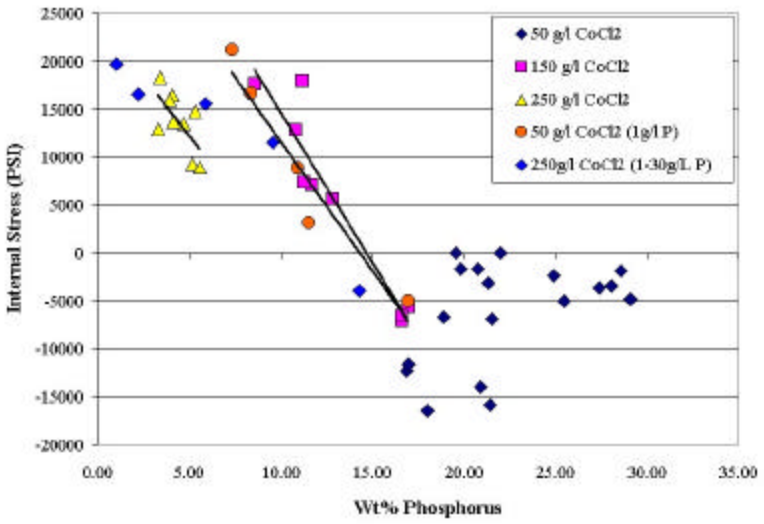

Figure 4-18 The internal stress of Co-P alloy electrodeposited coatings as a function of phosphorus concentration in the deposit.

4.6 Surface Roughness

The as-deposited surface roughness of nanocrystalline Co-P coatings has been investigated as a function of substrate surface roughness and/or current density. The study determined the levelling/roughening characteristics of nanocrystalline Co 2-3wt% P coating on mild steel samples with various initial surface roughnesses for various coating thicknesses and current densities. Nanocrystalline Co 2-3wt% P coatings were electroplated onto mild steel coupons (2"x 3") using the standard Co-P bath chemistry and plating conditions. The steel samples were mechanically ground and/or polished using different grit SiC abrasive paper (60, 240 and 100grit) to achieve different starting surface roughness. Coatings were applied using two different average current densities, 150 and 200 mA/cm^2 to thicknesses of 50, 100 and 250µm. The surface roughness of the samples was measured (in triplicate for each specimen) before and after coating using a Mitutoyo SJ-400 stylus profilometer.

The results of the surface roughness study are summarized in Tables 4-7 and 4-8 and Figures 4-19 and 4-20.

Table 4-7 Surface roughness of mild steel before and after coating with nanocrystalline Co 2-3wt%P with different thickness, using an average current density of 150mA/cm^2.

Surface Finish	**Surface Roughness, Ra (µm)**			
	Before Plating	After Plating		
		(50µm)	(100µm)	(150µm)
60 grit	0.94	0.87	0.88	0.76
240 grit	0.25	0.22	0.22	-
1000 grit	0.11	0.09	0.08	0.09

Table 4-8 Surface roughness of mild steel before and after coating with nanocrystalline Co 2-3wt%P with different thickness, using an average current density of 200mA/cm^2.

Surface Finish	**Surface Roughness, Ra (µm)**			
	Before Plating	After Plating		
		(50µm)	(100µm)	(150µm)
60 grit	1.23	1.16	1.02	1.04
1000 grit	0.12	0.09	0.11	0.09

The application of nanocrystalline Co-P coatings to mild steel does not significantly alter the starting surface roughness of the substrate being coated. The surface roughness of the coating was found to be very similar to the starting surface roughness of the substrate. In the case of the mild steel specimens ground using 60-grit SiC abrasive paper (highest starting surface roughness), the surface roughness was found to slightly decrease with increasing coating thickness.

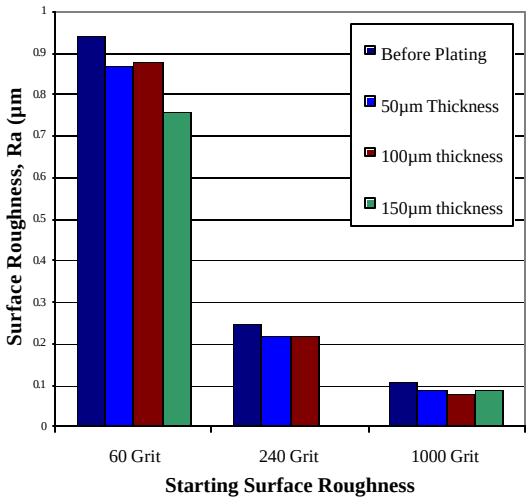

Figure 4-19 Surface roughness of 4130-steel with different starting surface roughness before and after applying nanocrystalline Co 2-3wt%P coatings (using an average current density of 150mA/cm^2) with different thickness.

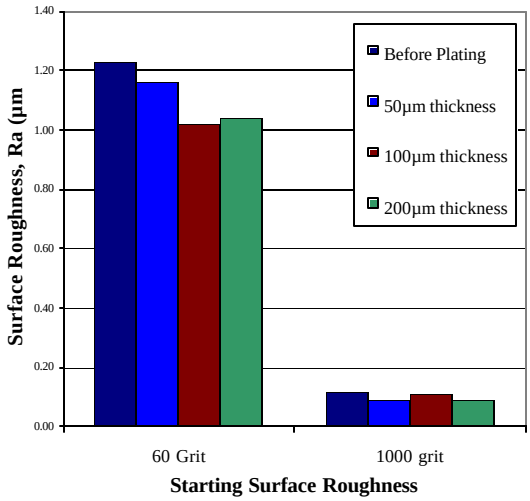

Figure 4-20 Surface roughness of 4130-steel with different starting surface roughness before and after applying nanocrystalline Co 2-3wt%P coatings (using an average current density of 200mA/cm^2) with different thickness.

4.7 Hydrogen Embrittlement

Hydrogen embrittlement specimens, fabricated from 4340 steel, were obtained from Smith & Williston with the Standard F-519 Type 1a notched bar specimen dimensions as shown in Figure 4-21. The test specimens were heat-treated to achieve R_c hardness of 48-50 before coating. Approximately 3 inches of the gauge length was coated with nanocrystalline Co-P, roughly 1 inch from the ends of the gauge length. The samples were plated four (4) at a time.

For the hydrogen embrittlement tests nanocrystalline Co-P coatings, with a phosphorus concentration between 2-3wt%, were deposited onto the standard notched hydrogen embrittlement specimens. The thickness of the coatings was approximately 0.004 inches. Twelve (12) specimens were coated, 4 of which were tested as deposited and 8 of which were tested after heat treatment at 191°C: four (4) after 12 hours and four (4) after 36 hours. The samples were heated-treated within 2 hours after plating.

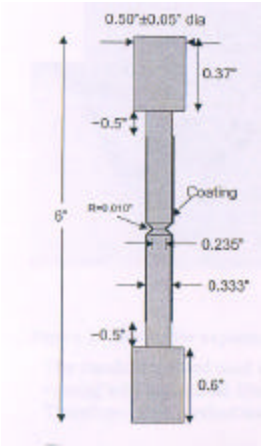

Figure 4-21 Standard F-519 hydrogen embrittlement specimens.

Figure 4-22 shows cross sections of a hydrogen embrittlement specimen plated with nanocrystalline Co 2-3wt%P at 200mA/cm^2 for 30 minutes. The thickness of the coating was approximately 25µm at the base of the notch (0.001") and 80µm on the edge (0.0032"). The surface of the plated specimen was smooth and shiny, with the occasional small nodule.

Two batches of Hydrogen embrittlement samples were tested. The results from the first batch were inconclusive, due to the questionable quality of the samples (the hardness of some the test samples was not as specified). For the second batch of samples, the hardness of each sample was measured prior to coating and only those that met the specification were coated. Additional test specimens were coated with hard chrome and tested in the as-deposited and baked condition. A summary of the hydrogen embrittlement test results for 4340 steel coated with nanocrystalline Co 2-3wt%P and Hard Chrome is given in Table 4-9.

Hard chrome specimens, tested in the as-deposited condition, failed within the first hour of testing, indicating severe hydrogen embrittlement has occurred. Samples tested after a bake-out procedure had been performed as per Mil-Spec-1501C showed no indication of embrittlement.

Nanocrystalline Co 2-3wt%P coated test samples tested in the as-deposited condition and after baking for 12 and 36 hours at 191°C showed **no indication of hydrogen embrittlement**.

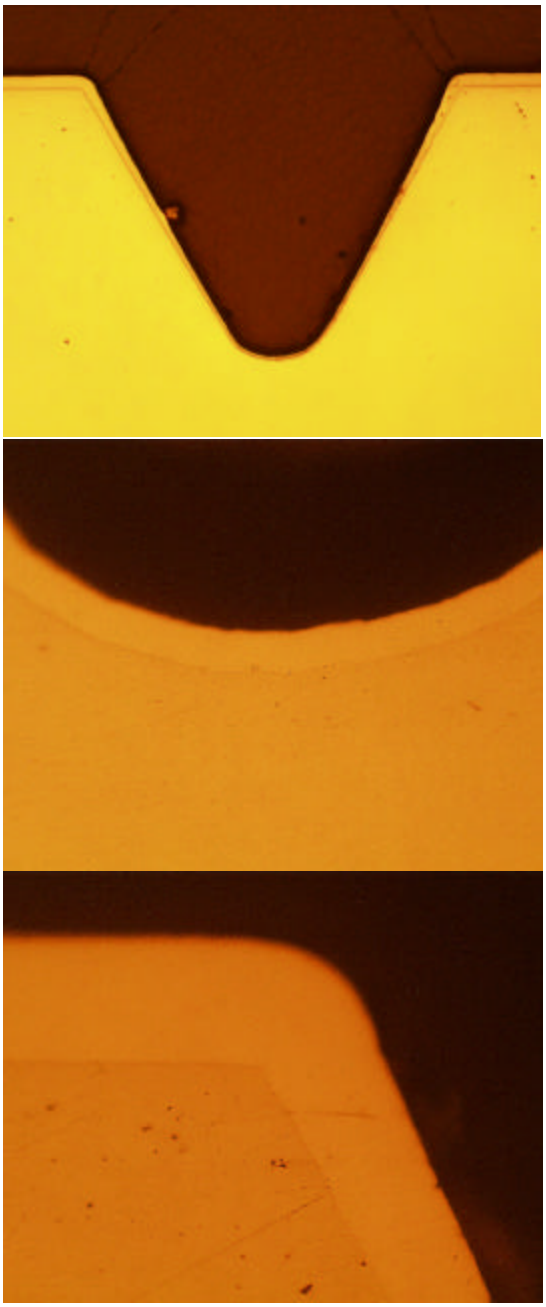

Figure 4-22 Optical micrographs of nanocrystalline Co-P in notch of F-519 specimens. From top to bottom: entire notch area; at bottom of the notch; and at the top edge of the notch.

Table 4-9 Summary of hydrogen embrittlement test results.

Coating	Bake Condition	Hours at 75% NFS	Failure % of NFS	Pass / Fail
Nanocrystalline Co 2-3wt%P	**No Bake**	205	90	Pass
		208	90	Pass
		203	75	Pass
		205	90	Pass
	12 hours, 191°C	234	85	Pass
		212	90	Pass
		208	90	Pass
		242	90	Pass
	36 hours, 191°C	212	90	Pass
		209	90	Pass
		242	85	Pass
		208	90	Pass
Electrolytic Hard Chrome	**No Bake**	0.5	75	Fail
		1.0	75	Fail
		Not Tested	-	-
		Not Tested	-	-
	24 hours, 191°C	200	90	Pass
		211	90	Pass
		233	90	Pass
		213	90	Pass

4.8 Uniaxial Fatigue Testing

Hourglass fatigue specimens with 0.25-inch gauge diameter were obtained from Metcut Research Associates Inc. The specimens were fabricated from 4340-steel and heat-treated to a tensile strength of 260-280 ksi. Some samples were shot peened over the entire surface of the specimen with a 100% surface coverage. A schematic of the specimens is shown in Figure 4-23.

The testing matrix is given in Table 4-10, which included samples coated with various nanocrystalline Co-P alloy coatings as well as samples coated with electrolytic hard chrome and uncoated samples for reference. Electrolytic samples were coated by FMI in Georgetown, Ontario to Mil-Std-1501C. Samples coated with nanocrystalline Co-P alloys were tested in two batches.

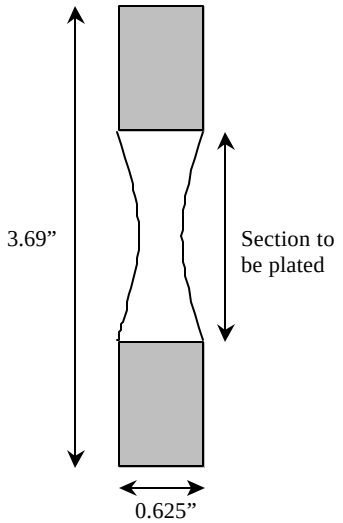

Figure 4-23 Schematic of the fatigue test specimens.

For the case of the Co-P coating, prior electrodeposition the specimens were grit blasted with either 80-grit (batch 1) or 120-grit (batch 2) aluminium oxide at 60-psi at 90-degree angle of impingement using a uniform standoff distance. Nanocrystalline cobalt-phosphorous coatings were deposited onto the surface of the specimens with no interfacial layer between the specimen and the coating. The coatings were deposited to approximately 0.006" in thickness and will be subsequently ground to a thickness of 0.003" +/- 0.0005", with a surface finish of 16µinches using low-stress grinding techniques in accordance with specification MIL-STD-866 prior to fatigue testing. Following plating, the samples were baked at 191°C for either 24 hours (batch 1) or 36 hours (batch 2).

Fatigue testing of the specimens was conducted according to the ASTM Standard E466 – Force Controlled Fatigue at McDermott Technology, Inc. under the supervision of Bruce Young. Testing was conducted at room temperature in lab air according to the matrix listed in Table 4-10. All testing was conducted at an R-Ratio of –1. A target frequency of 5 Hz will be used for stress levels of 175 and 150 ksi and a frequency of 20 Hz with stress levels of 125 and 110 ksi.

Table 4-10 Fatigue Test Matrix.

Coating	Batch	Peen	Stress Level			
			110 ksi	125 ksi	150 ksi	175 ksi
Bare	1	No	✔	✔	✔	✔
	1	Yes	✔	✔	✔	✔
Hard Chrome	2	No	✔	-	✔	-
	2	Yes	✔	✔	✔	✔
Nano Co	1	Yes	-	✔	-	✔
Nano Co 2-3wt%P	2	No	✔	-	✔	-
	1	Yes	-	✔	-	✔
	2	Yes	✔	✔	✔	✔
Nano Co 4-5wt%P	1	Yes	-	✔	-	✔
Co 15-20wt%P	2	Yes	✔	-	✔	-

Figure 4-24 shows the fatigue results (S/N curve) for the bare and electrolytic hard chrome 4340-fatigue test specimens. Figure 4-25 shows that for the various Co-P alloy coated specimens along with hard chrome coated peened-4340 specimens for comparison purposes. From the two curves it is evident there is a reduction in fatigue life for 4340-specimens with Co-P alloy coatings for samples tested at low stress levels (110, 125 and 150 ksi) but not at the high stress level (175 ksi). A reduction in fatigue life for 4340-specimens coated with hard chrome, however, was evident at all stress levels. SEM examination of the fracture surface of hard chrome and various Co-P coated samples showed no significant abnormal features that accounted for the reduction in fatigue life. Figures 4-26, 4-27 and 4-28 show SEM micrographs of typical fracture surfaces found in bare, hard chrome and Co 2-3wt%P coated 4340-fatigue samples (peened), respectively.

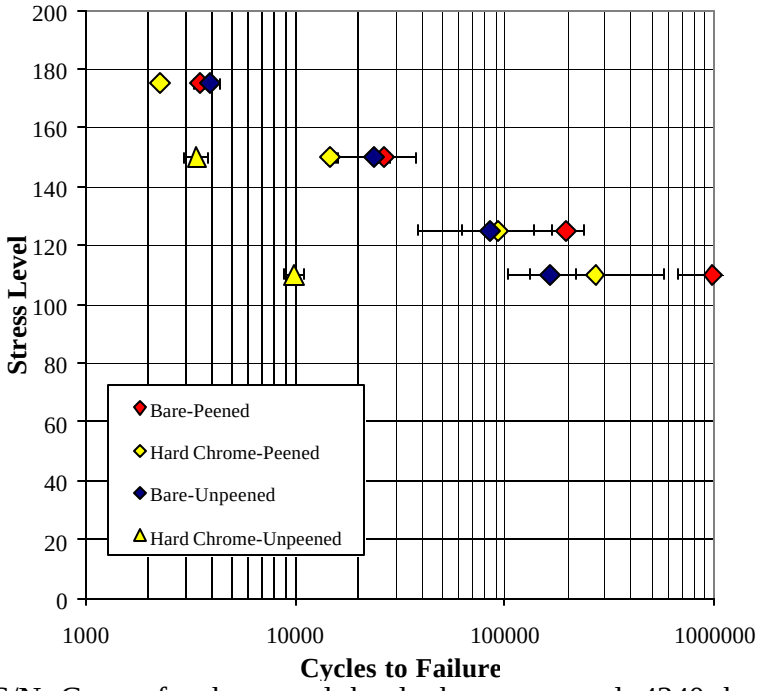

Figure 4-24 S/N Curve for bare and hard chrome coated 4340 hourglass fatigue specimens in the peened and un-peened condition.

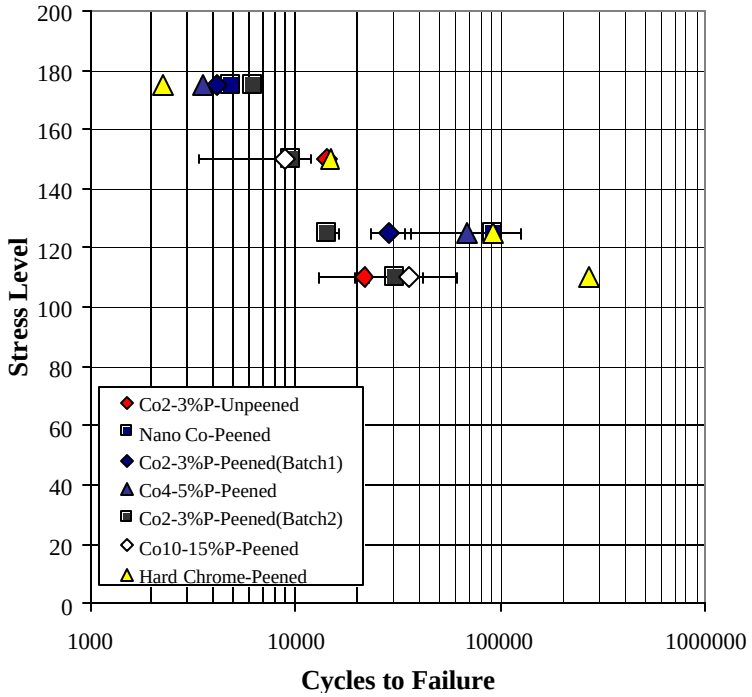

Figure 4-25 S/N Curve for various nanocrystalline cobalt-phosphorus alloy coated 4340 hourglass fatigue specimens in the peened and un-peened condition along with hard chrome coated specimens for reference.

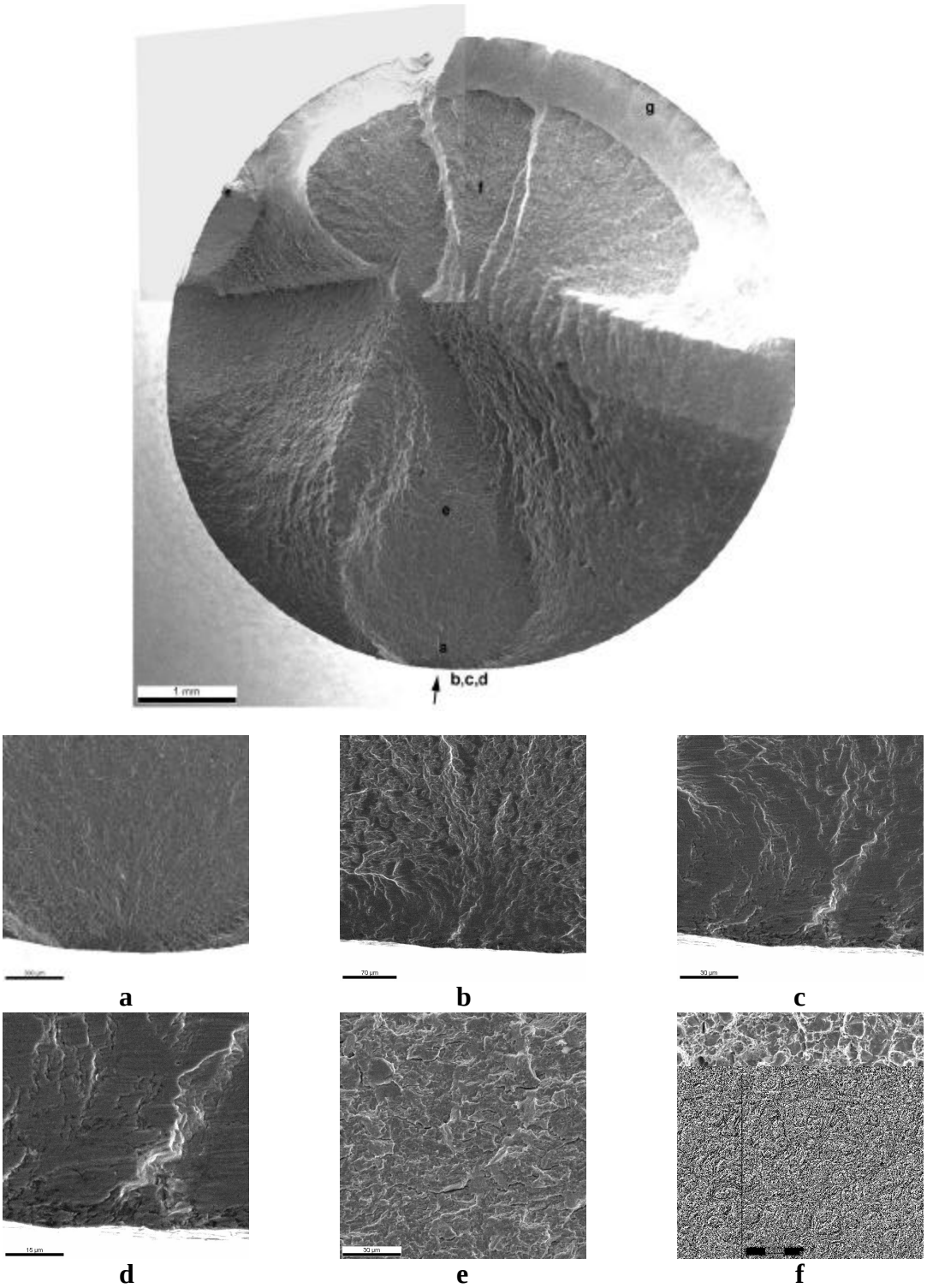

Figure 4-26 SEM micrographs of a typical fracture surface and various locations on the fracture surface of an uncoated 4340-fatigue specimen (peened) tested at a stress level of 125 ksi.

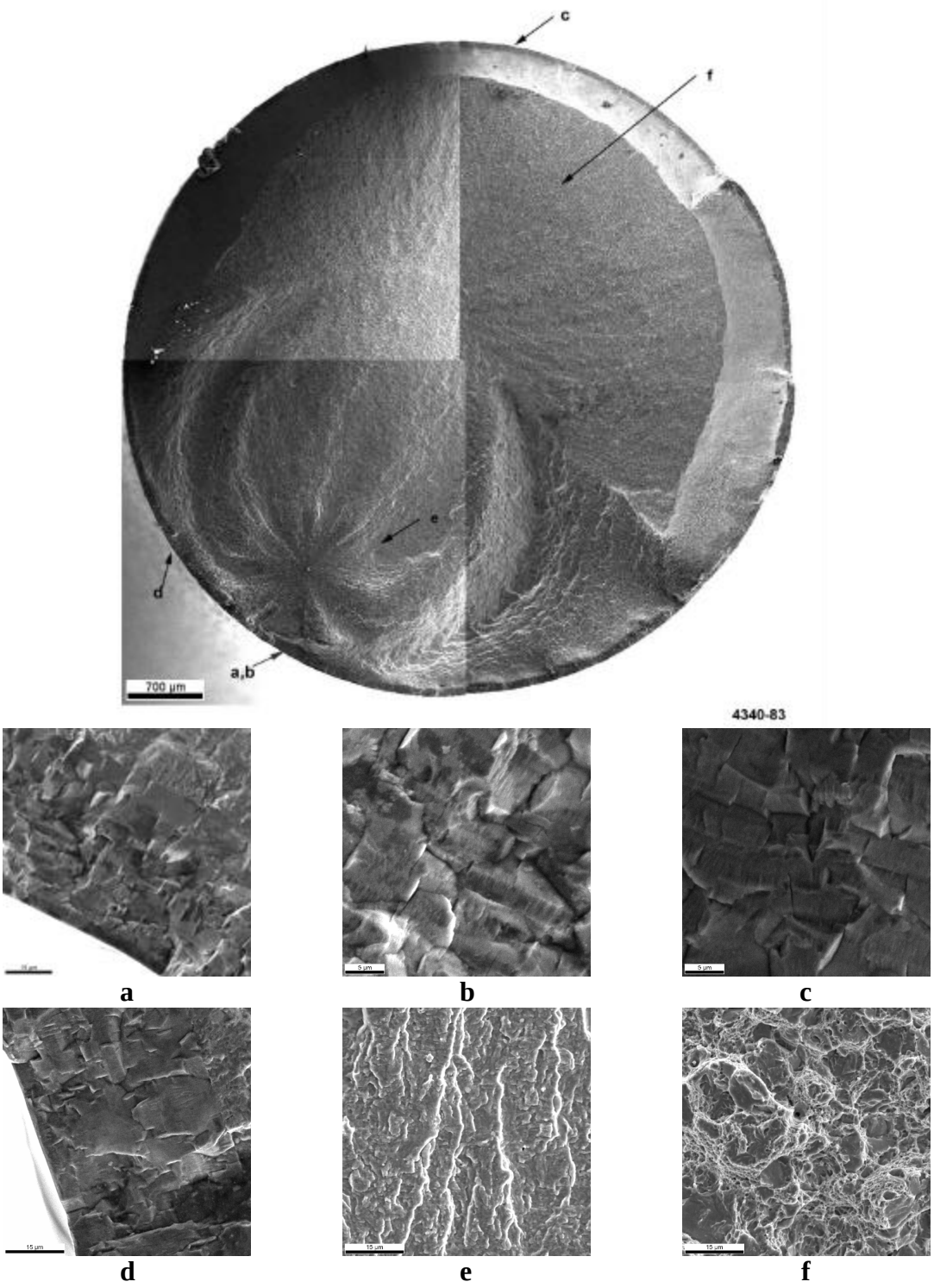

Figure 4-27 SEM micrographs of a typical fracture surface and various locations on the fracture surface of an electrolytic hard chrome coated 4340-fatigue specimen (peened) tested at a stress level of 110 ksi.

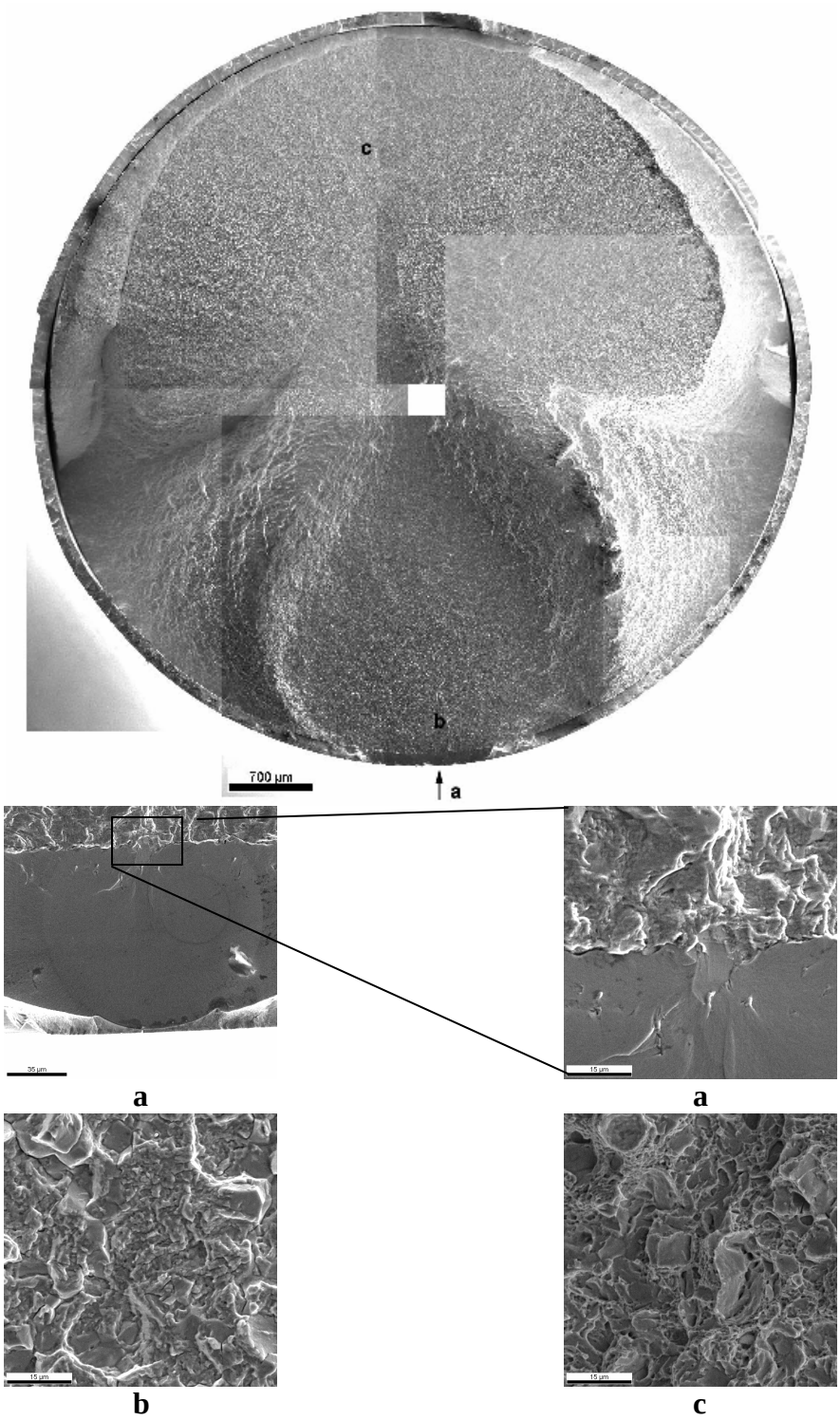

Figure 4-28 SEM micrographs of a typical fracture surface and various locations on the fracture surface of a Co 2-3wt% coated 4340-fatigue specimen (peened) tested at a stress level of 110 ksi.

Close examination of the interface between hard chrome coating and the base metal revealed a very smooth interface with many small fatigue cracks extending from the coating into the base metal, as seen in Figure 4-29. The presence of the many small cracks, originating in the micro-cracked chrome coating that extend into the base metal, may be the cause of the reduced fatigue life over the uncoated fatigue samples.

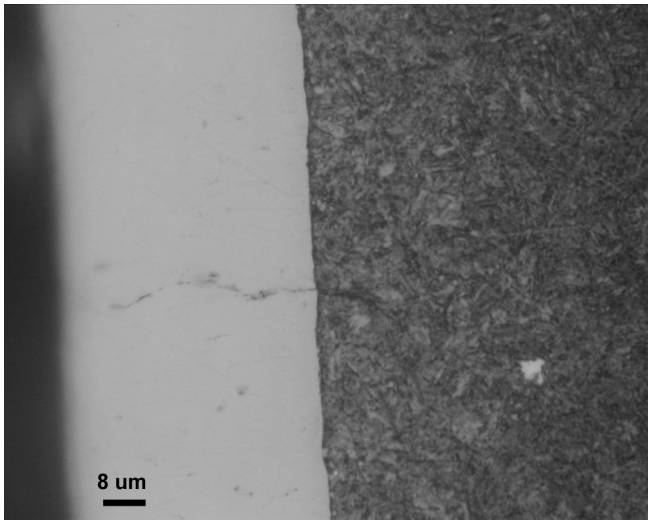

Figure 4-29 Optical micrograph of a cross-section showing the interface between the hard chrome coating and the base metal of a hard chrome coated 4340-fatigue specimen (Peened).

Examination of the interface between Co-P alloy coatings and the base metal revealed a very rough interface, with, in some cases, Alumina oxide particles trapped in the surface (residue from sand blasting during the cleaning step prior to electroplating). Figure 4-30 shows an optical micrographs of the coating/base metal interface of nanocrystalline Co 2-3wt%P and Co 15-20wt%P coated fatigue samples, showing a very rough surface. Figure 4-31 shows SEM micrographs of the coating/base metal interface of nanocrystalline Co 4-5wt%P coated fatigue samples showing indications of trapped Al_2O_3 particles. EDX analysis was performed on the particles to confirm that the composition of the particles matched that of Alumina.

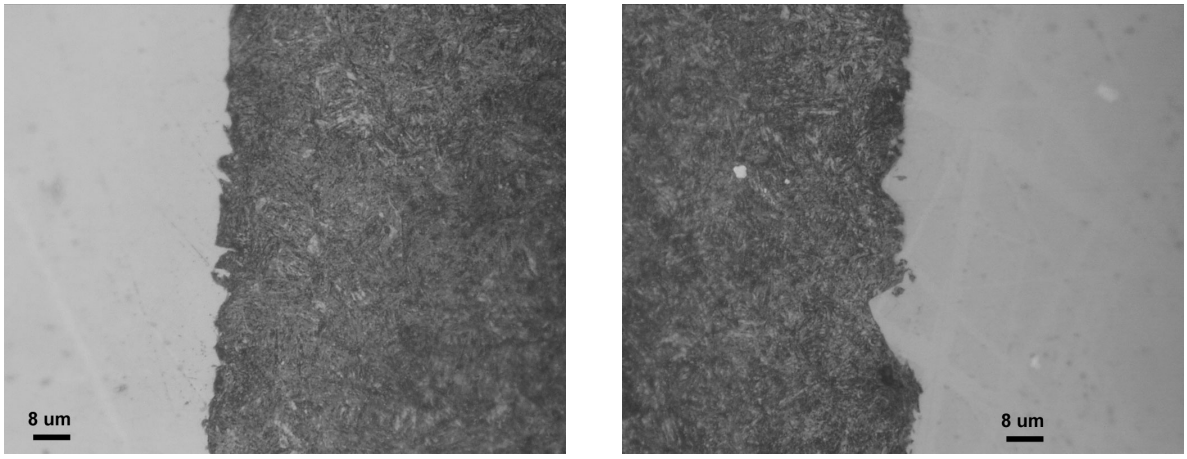

Figure 4-30 Optical micrograph of a cross-section showing the interface coating/base metal interface between a) nano Co 2-3wt%P and b) Co 15-20wt%P coatings on 4340-fatigue specimens (Peened).

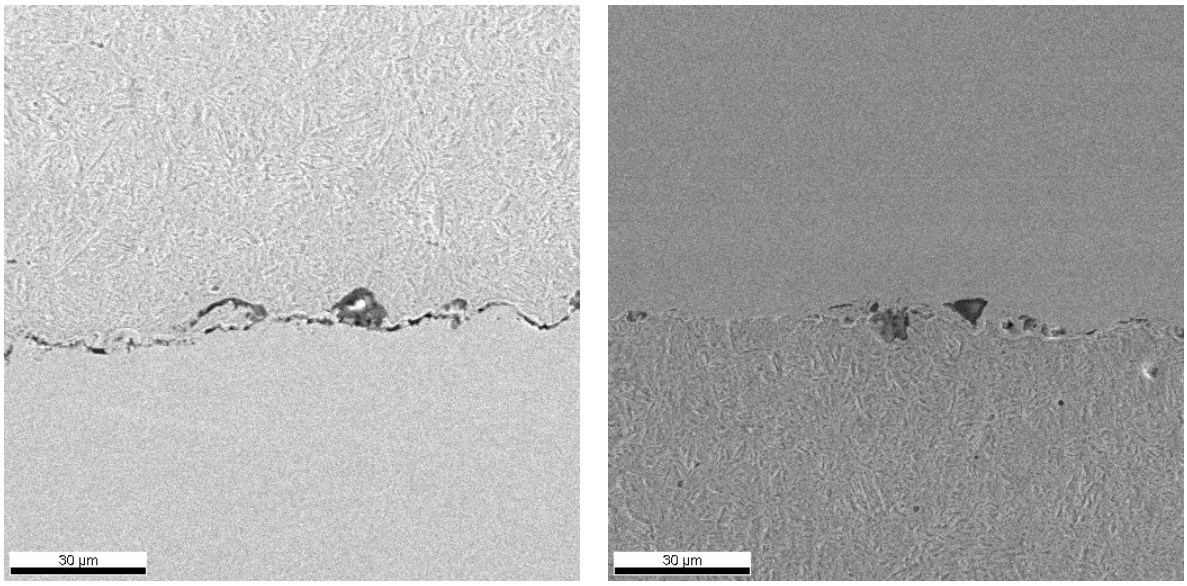

Figure 4-31 SEM micrographs of cross-sections through 4340-fatigue specimens (Peened) coated with nano Co 4-5wt%P showing a very rough interface with trapped alumina particles.

The very rough surface, along with the presence of trapped alumina oxide particles found on the coating/base metal interface of the nanocrystalline Co-P alloy coated fatigue samples is the most probable the reason for the reduction in fatigue life. Both the rough surface and/or the particles would act as stress concentrators, which would significantly increase the probability of fatigue crack initiation.

As the nanocrystalline Co-P coatings have been shown to be free of cracks pits and/or pores, have reasonable ductility, and have not been found to cause hydrogen embrittlement in high strength 4340 steel, there is no expectation that the coating should result in a fatigue debit. The rough surface and the presence of alumina particles on the surface of the nanocrystalline Co-P coated fatigue samples severely jeopardized the fatigue performance, producing results that are not indicative of the true nature of the coating. Therefore the fatigue tests have to be repeated, taking steps to ensure that the surface of the fatigue specimens are clean and smooth prior to coating.

5.0 APPLICATION TO INTERNAL DIAMETER SURFACES

5.1 DESCRIPTION OF MOCK-UP GEOMETRIES

The application of nanocrystalline cobalt-phosphorus alloy coatings has been aimed for the replacement of hard chrome coatings on the internal diameter (ID) of aerospace components where the ID is too small to employ HVOF coatings. In a recent report investigating various chrome replacement technologies for internals and small parts, the following geometries were found to be problematic for HVOF coatings:

- Holes (blind and through) in hydraulics, including landing gear and actuators
- Pins, such as those used in landing gear and actuators
- Lugs and other items where the coating is external, but access to the area is difficult

Figures 5-1, 5-2 and 5-3 show diagrams of aerospace components in which the ID surface is typically hard chrome plated. Figure 5-1 shows a cross section commonly found in landing gear outer cylinders, Figure 5-2 shows a 4" long, 1" diameter landing gear pin and Figure 5-3 shows a landing gear lug.

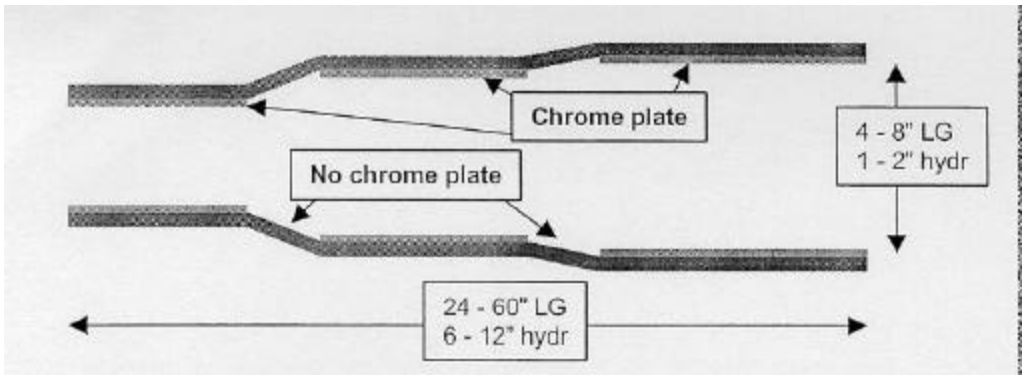

Figure 5-1 Complex landing gear outer cylinder cross-section schematic.

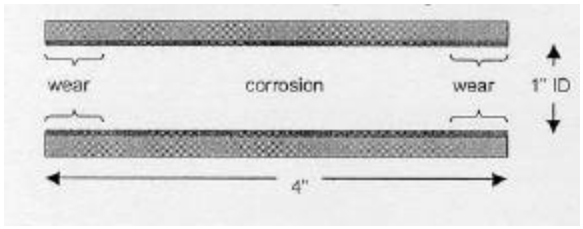

Figure 5-2 Landing gear pin – ID chromed.

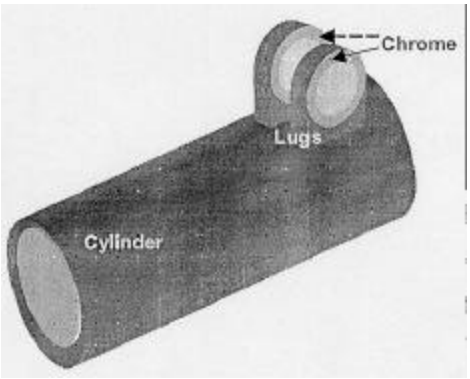

Figure 5-3 Schematic of a landing gear lug.

Four mock-up geometries were designed (see figures 5-4 and 5-5), duplicating these geometries as closely as possible. The four geometries include: a 6" long 1" diameter open ended cylinder, a 12" long 4" diameter close ended cylinder, two mock-up's (different diameters) of the landing gear outer cylinder shown in figure 5-1, and a mock-up of landing gear lugs.

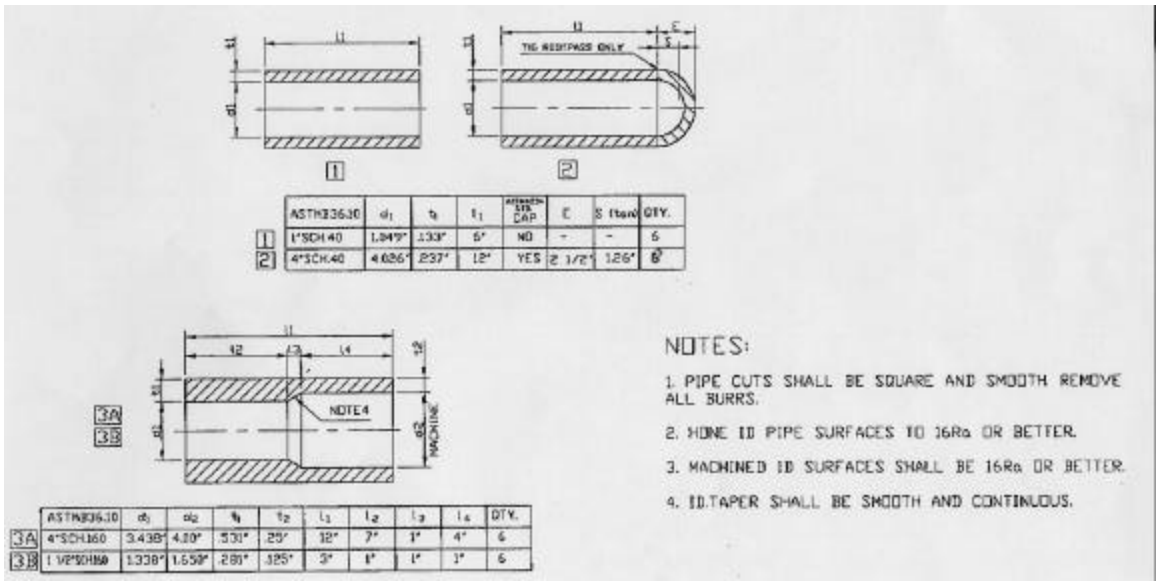

Figure 5-4 Schematic of cylindrical ID Plating Mock-Up.

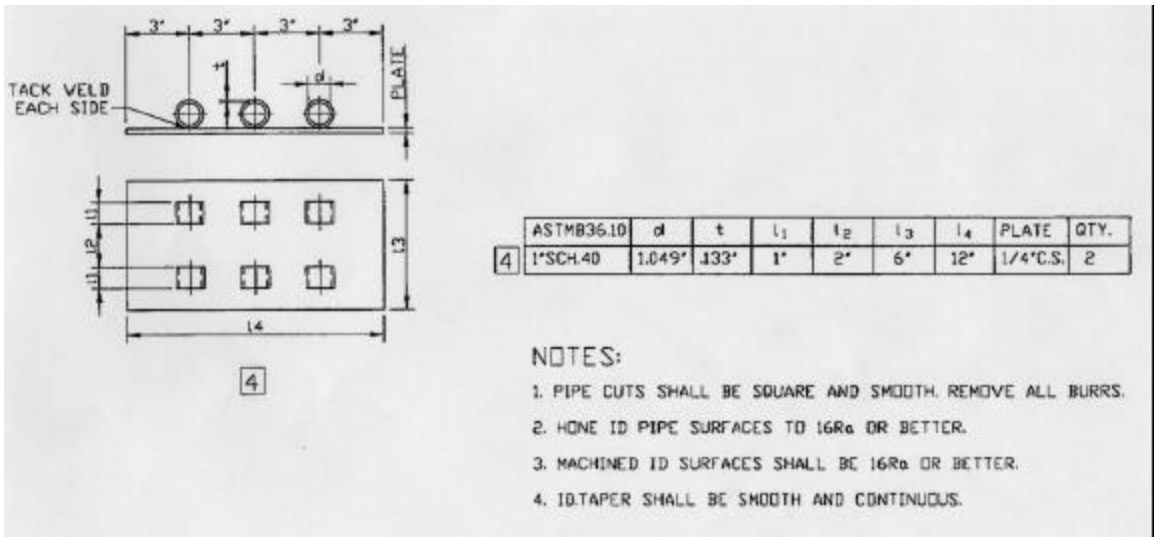

Figure 5-5 Schematic of Lug ID plating mock-up.

5.2 ONE-INCH DIAMETER PIPE (ID1)

Nanocrystalline Co-P deposits were electroplated onto the internal diameters of one-inch diameter pipes using the standard cobalt-phosphorous plating solution. Figure 5-6 shows the jig designed to fit onto Schedule 30 pipe (1 inch diameter). The function of the jig is to allow fresh plating solution to be pumped through the pipe and to hold the anode in the centre of the pipe and was used to plate the first mock-up geometry shown in Figure 5-4. Both consumable and non-consumable anodes were investigated using this set-up. The consumable anode was a polycrystalline cobalt plated platinum anode, and two non-consumable anodes studied were a 1/8th inch diameter platinum rod and a ¼ inch diameter graphite rod.

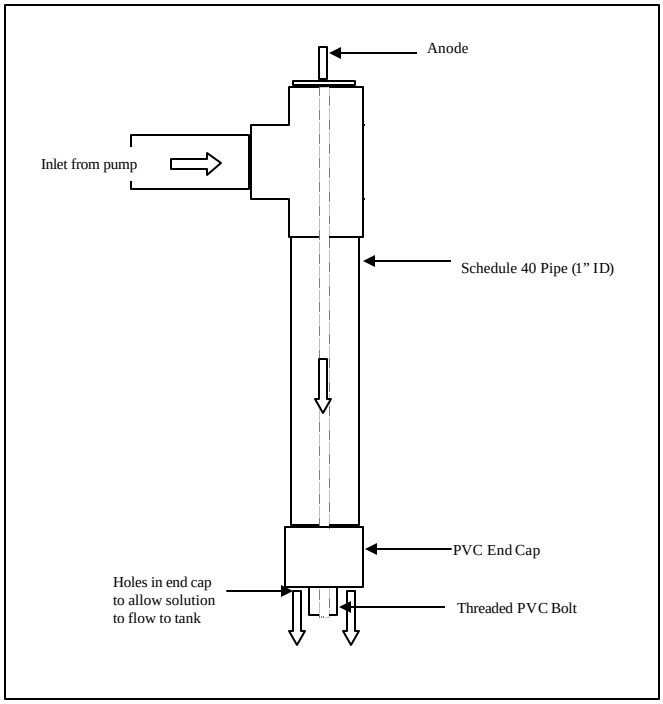

Figure 5-6 Schematic of jig to plate the ID of schedule 40 (1 inch low carbon steel pipe).

5.2.1 Consumable (Cobalt) Anode

A consumable cobalt anode, made by electroplating approximately 150µm (0.006") of polycrystalline cobalt onto a platinum anode was employed during the deposition process. The ID of a 1-inch pipe ID was successfully plated provided the flow through the plating jig was constant. Figure 5-7 shows a cross-section of the nanocrystalline coating taken at the middle of plate. A coating thickness of approximately 75µm was obtained by plating for 1 hour. In order to obtain uniform coating thickness around the entire circumference the anode must be properly centred. For the case of using a cobalt coated platinum rod it is important that the platinum is not exposed at any point during plating. This will cause an unsatisfactory coating to be deposited.

5.2.2 Non-consumable (Graphite) Anode

The ID's of numerous 1-inch pipes were plated with nanocrystalline Co-P using a ¼ inch graphite anode using the standard Co-P plating solution. Figures 5-8 and 5-9 show typical cross-sections of Co-P deposits plated for 1-hour and 4-hours, respectively. Both figures show a well-adhered, structurally sound coating. The graphite anode was found to produce very satisfactory deposits. With the use of a non-consumable graphite anode, a pH drop was expected due to the evolution of oxygen at the anode. A significant drop in the pH, however, was not noticed in the bath after the ID plating runs, most likely due to the relatively large volume of solution (20L) for the area plated (110cm^2). The graphite anode did not appear to significantly degrade after each run. After approximately 30 Ampere-hours of plating with the graphite anode, the chloride-based bath chemistry was found to produce satisfactory deposits.

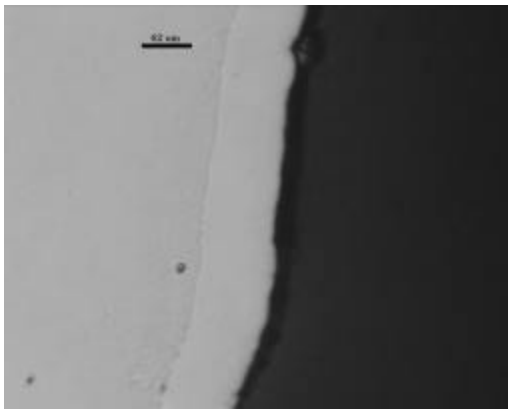

Figure 5-7 Nanocrystalline Co-P plated on the ID of a one-inch pipe using a consumable cobalt anode.

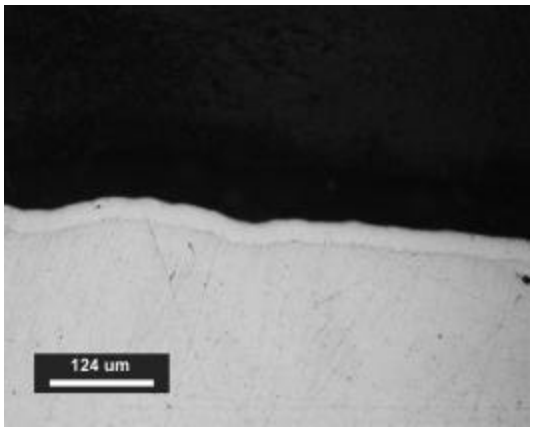

Figure 5-8 Nanocrystalline Co-P plated on the ID of a one-inch pipe for 1-hour using a non-consumable graphite anode.

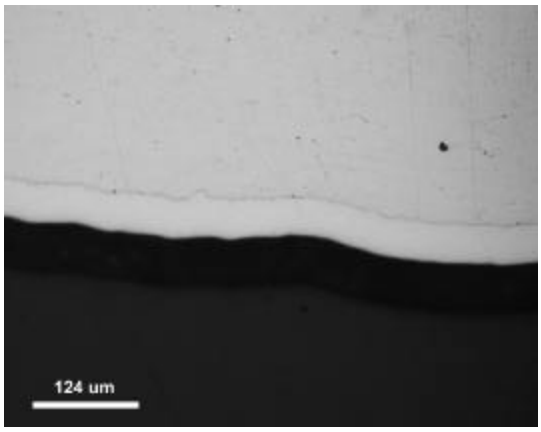

Figure 5-9 Nanocrystalline Co-P plated on the ID of a one-inch pipe for 4-hours using a non-consumable graphite anode.

5.3 FOUR INCH DIAMETER PIPE (ID2)

5.3.1 Open Ended Pipe - ID2A

Nanocrystalline Co-P was electroplated onto the ID of Schedule 40 pipes (4" diameter) using the standard plating solution and the plating jig shown in Figure 5-10. The jig provided the same function as that for the one-inch pipe, and consists of two C-

PVC end caps with a fitting mounted in the centre in which either a 0.25" or 1" diameter graphite rod can be placed for use as the anode. Plating solution is pumped into the bottom of the set-up and is allowed to flow out of the top end cap.

5.3.1.1 Consumable (Cobalt) Anode

Two types of consumable cobalt anodes were used to plate opened ended 4-inch diameter pipes: a solid cobalt rod and cobalt pieces in a titanium basket. Both types were successfully used to deposit a good quality coating. The most important factors that were found to compromise the quality of the coating were the flow of solution through the pipe and the condition of the anode. It is essential that the flow of solution through the pipe is adequate or else the anode will overheat and cause the solution to boil. For the case of the basket anode, it is important that the anode is well bagged or else small particles from the dissolving anode may be co-deposited on the substrate cause excessive surface roughness.

Figure 5-10 Photograph of the plating jig to plate the ID of schedule 40 (4" diameter) pipe.

5.3.1.2 Non-consumable (1-inch Graphite) Anode

A one-inch non-consumable graphite anode was successfully used to deposit Co-P coatings on the ID of 4-inch pipe. The coating completely covers the entire substrate and is free of porosity. Figure 5-11 shows a cross-section of a typical coating plated for 3 hours. Due to the relatively large surface area and power requirements, the use of a non-consumable anode requires cobalt carbonate (to replenish Co^{2+} ions and maintain pH) and phosphorous acid (to replenish phosphorus) additions during plating to maintain coating integrity (see section 2-2). Hardness measurements and compositional analysis across the thickness of the sample that was plated

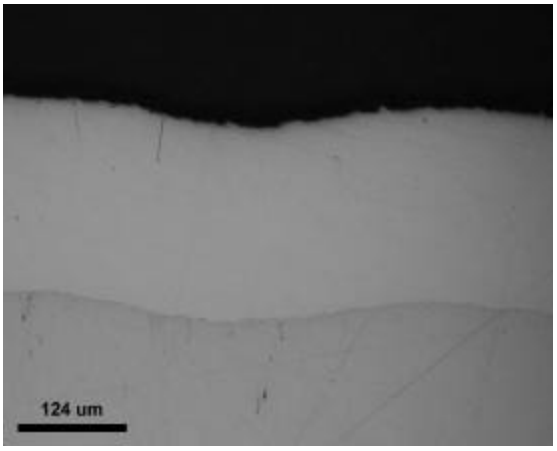

Figure 5-11 Nanocrystalline Co-P plated on the ID of a four-inch diameter pipe for using a non-consumable (1-inch diameter graphite) anode at 62mA/cm^2 for 3 hrs.

without bath additions during plating are shown in Table 5-1. The results show that the phosphorus concentration in the deposit dropped substantially through the course of the run, resulting in a corresponding drop in the hardness. The drop in phosphorous concentration is larger than would be expected if the incorporation of phosphorus into the deposit were the only reason for the decrease. Therefore it is suspected that a secondary reaction may be occurring which consumes the phosphorous acid in solution (see Section 2.2).

Table 5-1 Hardness at distance from deposit/substrate interface.

Distance From Interface	0µm	20um	40um	60um	80um	Outer Surface
Hardness (VHN)	540	530	490	440	410	345*
Wt%P	3.2	3.08	2.35	2.24	1.68	1.17

*hardness indentations were not square

5.3.2 Blind Hole Pipe - ID2B

A titanium anode-basket (shown in Figure 5-12), that holds cobalt pieces for use as a consumable anode, was designed to fit into the 4" diameter-plating jig described in section 5.3.1 and shown in Figure 5-10. This set-up pumps plating solution from the interior of the pipe through the centre of the anode, with fresh plating entering the pipe from holes around the top of the jig. With this set-up there is no impingement of plating solution on the surface of the substrate.

5.3.2.1 Consumable (Cobalt) Anode

The plating jig shown in Figure 5-12 was successfully used to deposit Co-P coatings on the ID of blind holed 4-inch diameter pipes. Similar to the case of the open-ended pipe, solution flow must be adequate to prevent anode overheating. A photograph of a typical deposit on the ID of the blind-hole pipe is shown in figure 5-13. The coating is typically uniformly bright over the entire surface. To maintain coating uniformity over the entire surface of the ID it is essential that the anode be well centred, with the end of the anode equally spaced between the bottom of the pipe and the sidewalls. Rotating the anode 45° every 15 minutes (for a total plating time of one hour) provided a very uniform coating along the entire circumference of the pipe.

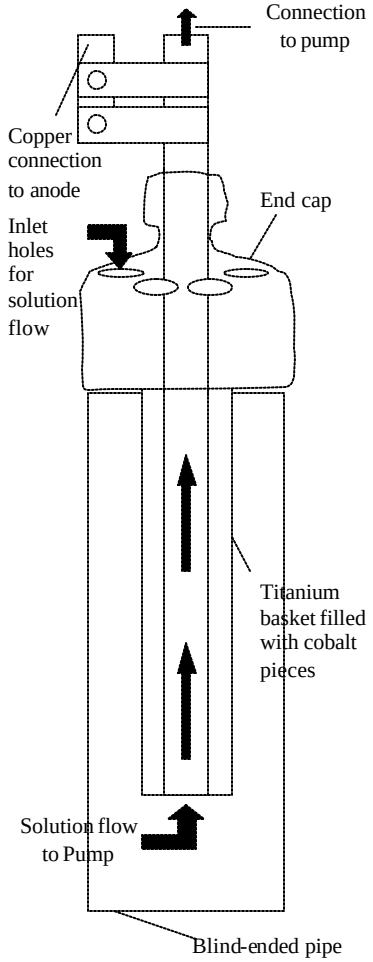

Figure 5-12 Photograph and schematic of the titanium-anode basket (covered with an anode bag) for plating the ID of 4-inch diameter blind hole pipes.

Figure 5-13 Photograph of the inside surfaces of a blind-holed 4-inch diameter pipe plated with nanocrystalline Co-P.

5.4 STEPPED DIAMETER PIPES

5.4.1 ID3B – Small ID

A schematic of the plating jig design to plate the small stepped ID geometry as described in section 5.1 is shown in Figure 5-14. To prevent deposition onto the tapered section of the stepped diameter pipe, a plastic block is used as a mask, with a dual purpose of centring the graphite anode. The end-caps also hold the anode in the centre, and allow fresh solution to flow through during plating when one of the end caps is connected to a pump.

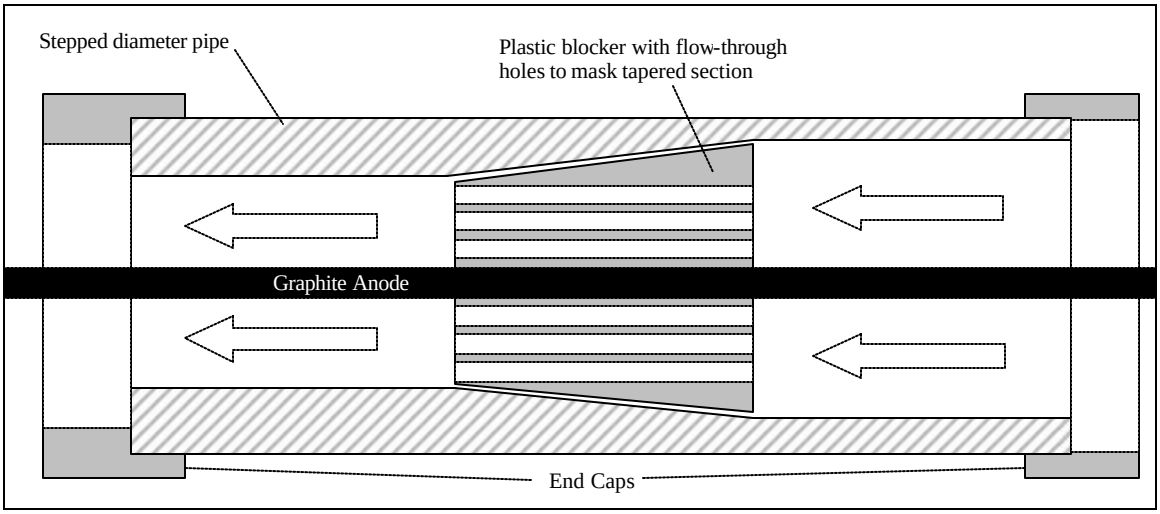

Figure 5-14 Schematic of the plating jig used to plate the ID of small stepped diameter pipes (ID#3B). Arrows indicate solution flow through the pipe.

Using the standard cobalt-phoshorus bath chemistry, mock-up sample ID#3b (small stepped ID) was successfully plated using a stepped graphite anode. The stepped anode was designed such that the distance between the cathode and anode for both ID surfaces was maintained constant. Figure 5-15 shows the plated sectioned sample along with the stepped anode. The sample was plated at 200mA/cm^2 using pulse conditions of T_{on}/T_{off} of 2/4ms, respectively for 45 minutes. Cross-sectional analysis of the coating shows that coating is approximately 0.005-0.006" thick and is uniform between the two sections.

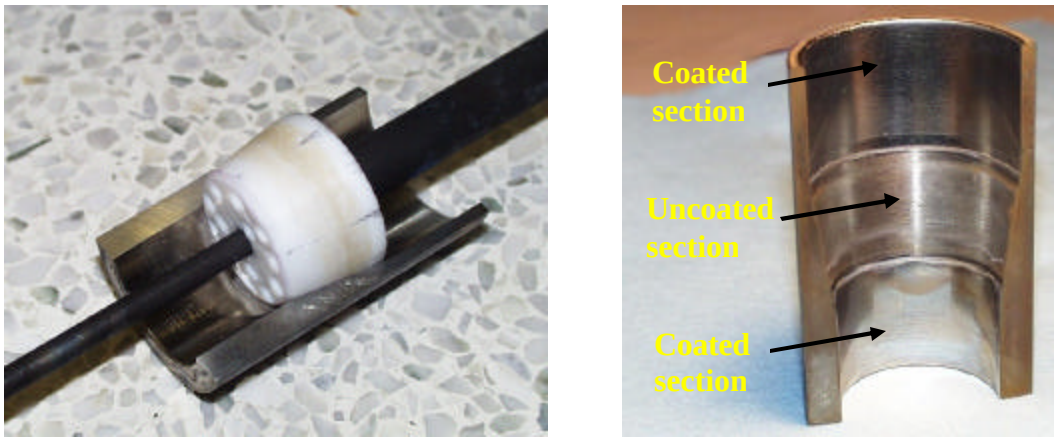

Figure 5-15 **(a)** Plated mock up sample ID3B (after sectioning) along with the plastic plug and the stepped graphite anode, **(b)** Photograph of the inside surface of a stepped ID (1.65/1.338inch) pipe showing coated and uncoated sections.

5.4.2 ID3A – Large ID

Large diameter stepped ID samples were successfully plated using the typical Co-P plating solution at using pulse conditions of T_{on}/T_{off} of 2/4ms, respectively at an average current density of 150mA/cm^2 for 60minutes. Runs were performed with a straight titanium anode filled with cobalt pieces, and with a change in diameter to maintain constant anode to cathode current density through the change in internal diameter in the sample. In both cases a plastic plug was inserted to mask off the surface centre portion of the sample (where the diameter changes) to prevent metal deposition.

Three runs were performed on the large stepped ID mock-up samples. The first used a straight consumable cobalt anode (no change in ID) and the coating thickness target was 5 mils. The second used a consumable cobalt anode that was taped to maintain a constant anode to cathode distance through the step in the sample ID and the target for coating thickness was 5 mils. The third run used the stepped anode and the target thickness was 2 mils. In all three cases the phosphorus concentration ranged between 2 and 2.5wt% and the average hardness was approximately 525 VHN. The hardness was lower than expected, but is believed to be the result of copper contamination in the bath from poorly covered copper wire used for the cathode connection. Table 5-2 shows the average thickness of the coating in the small and large ID section for the three runs. Figure 5-16 shows optical micrographs of cross-sections of the coatings at the large and small diameters of the three samples.

For the first run where the anode to cathode distance varied through the step, the difference in thickness is proportional to the variation in anode to cathode distance (~75-85%). For the second and third run where the anode to cathode distance was constant the thickness of the coatings on the large and small diameters are the nearly equivalent.

Table 5-2 Coating thickness of the ID3a (large stepped ID) mock-up samples.

ID Size	Location from End of Pipe	Thickness (µm)		
		Run 1	Run 2	Run 3
Large	4 cm	215	183	80
Large	14 cm	223	183	72
Small	22 cm	169	177	72
Small	28 cm	168	190	73

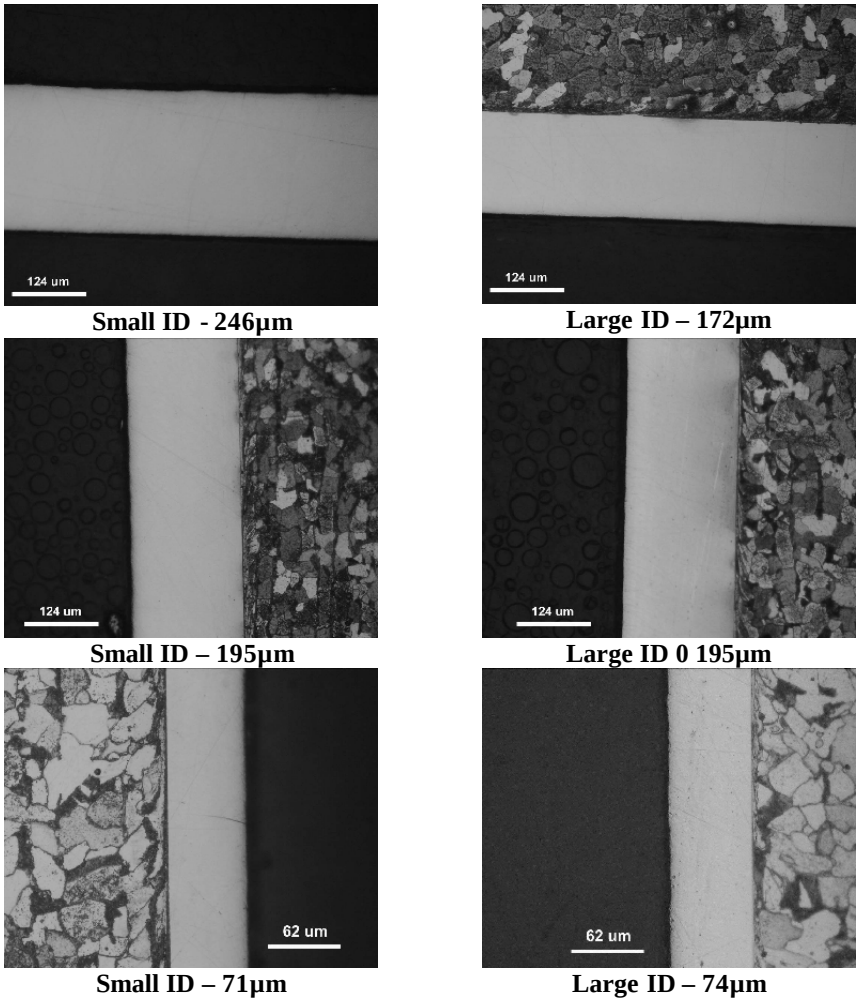

Figure 5-16 Optical micrographs of coating cross-sections on the small and large diameters, respectively, of samples ID3A-R1 to ID3A-R3.

5.5 LUGS - ID4

The internal diameter and faces of two one-inch diameter lugs welded to a steel plate were successfully coating with Co-P coating using the plate assembly shown in Figure 5-17. Due to the small diameter of the lugs, a ¼ inch diameter graphite anode was used. Un-plated areas were masked with tape. A slight overhang of tape was intentionally placed on the lug ends to discourage dendrite formation on the sharp edges of the lug edge face. With only a ¼ inch graphite anode running down the centre of the lugs, a thicker coating was obtained on the ID than on the lug face. This can be corrected by maintaining a constant distance between the all the plated surfaces and the anode. Figure 5-18 (a) and (b) show cross-sections of the coating on the ID and lug face, respectively.

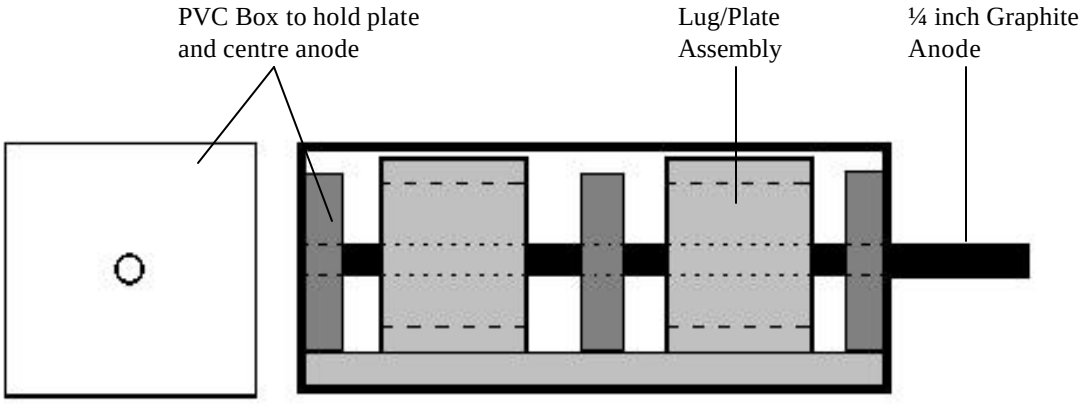

Figure 5-17 Schematic of the plating assembly used to hold the ¼ graphite anode in the centre of the lug/plate samples (ID4)

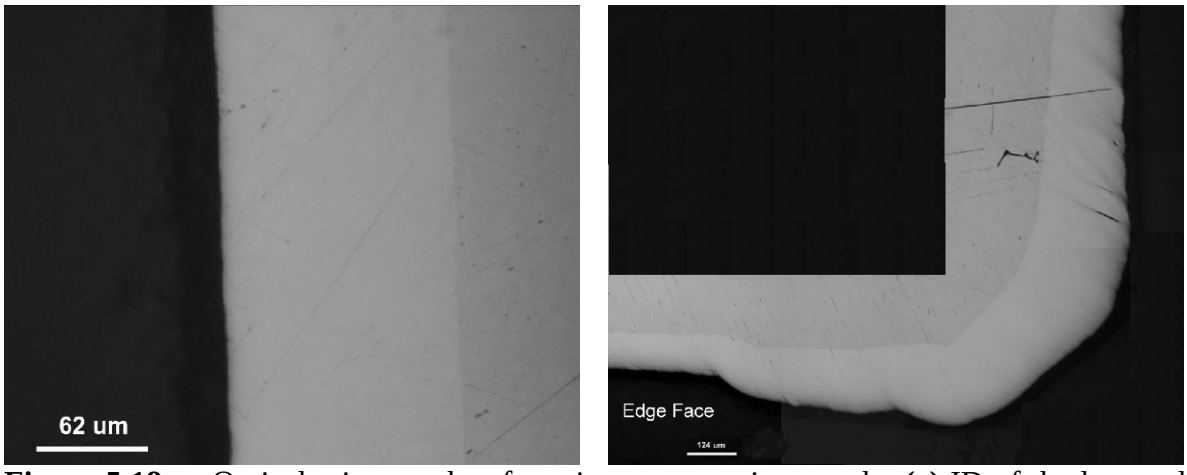

Figure 5-18 Optical micrographs of coating cross-sections on the **(a)** ID of the lug, and **(b)** face of the lug.

5.6 Final Demonstration Validation

As a final validation for the process, part of the internal diameter surface of a shock strut of a landing gear assembly (provided courtesy of Messier-Dowty Aerospace) was coated with nanocrystalline Co 2-3wt%P. The coated section was the bottom 2¼" of internal diameter surface. The total length of the part was approximately 20". Following the basic design concepts developed in sections 5.2 through 5.5, a suitable anode basket and plating assembly was designed with the purpose of centring the anode in the part and holding it in place at the same time as masking the uncoated areas. Schematics of the anode basket, top end cap and bottom end cap are shown in Figures 5-19 and 5-20, respectively.

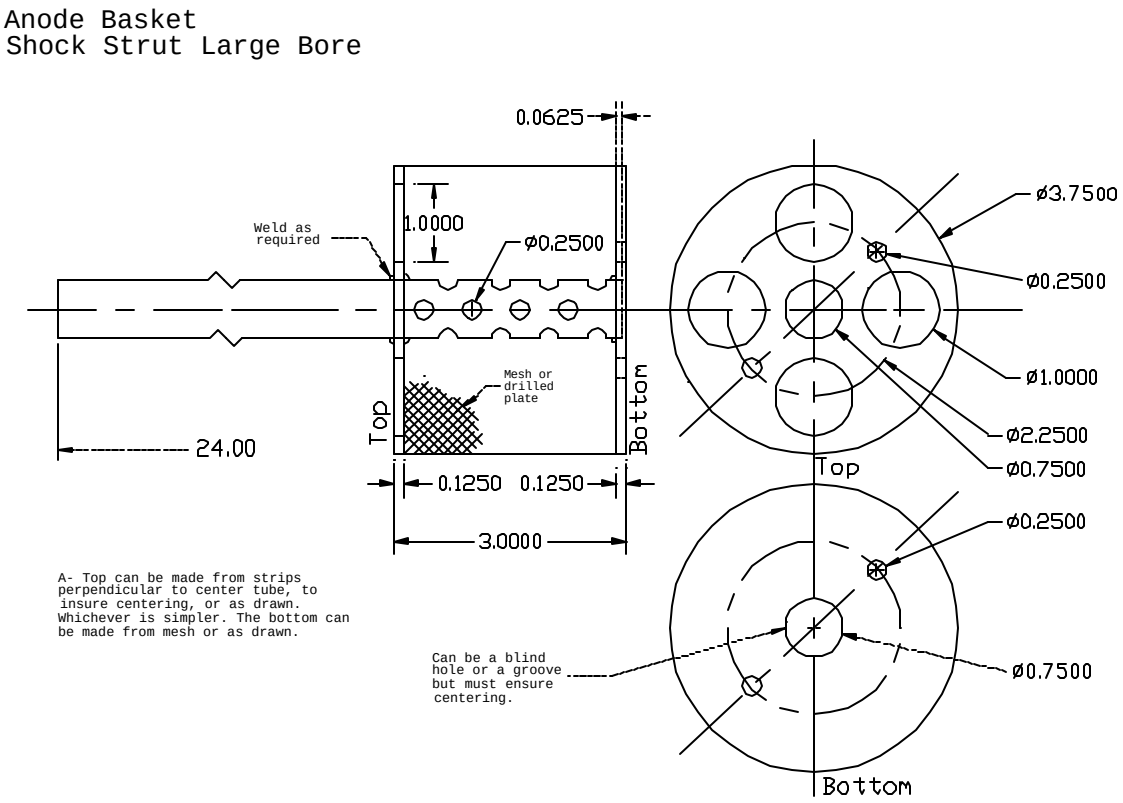

Figure 5-19 Schematic of the anode basket used to plate the internal diameter surface of a shock strut component of a landing gear assembly.

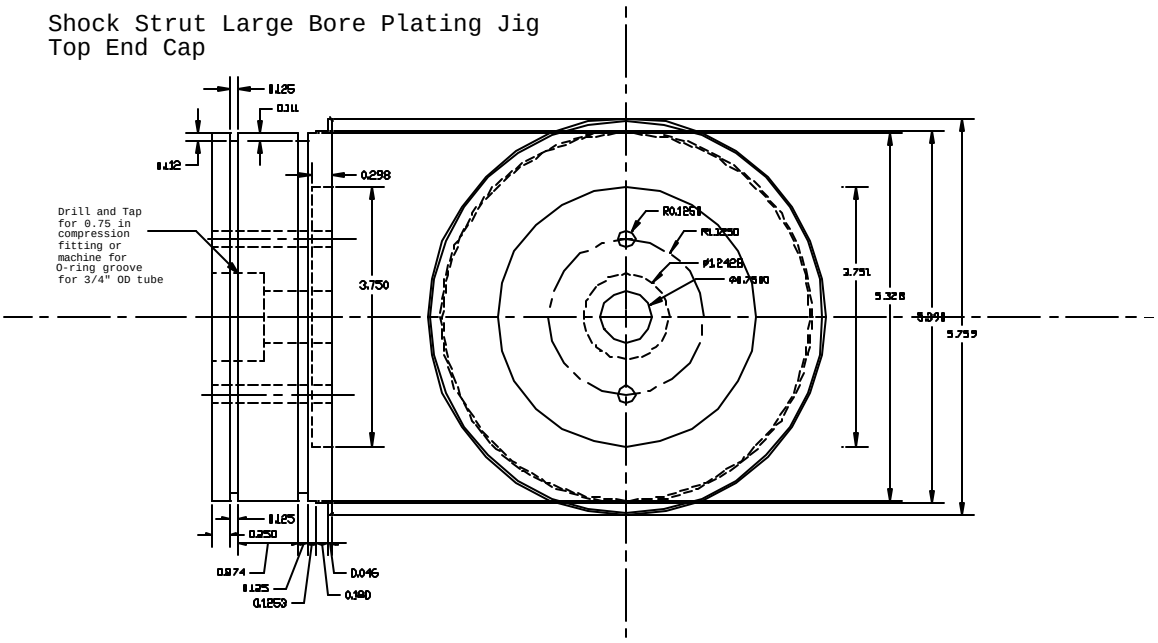

(a)

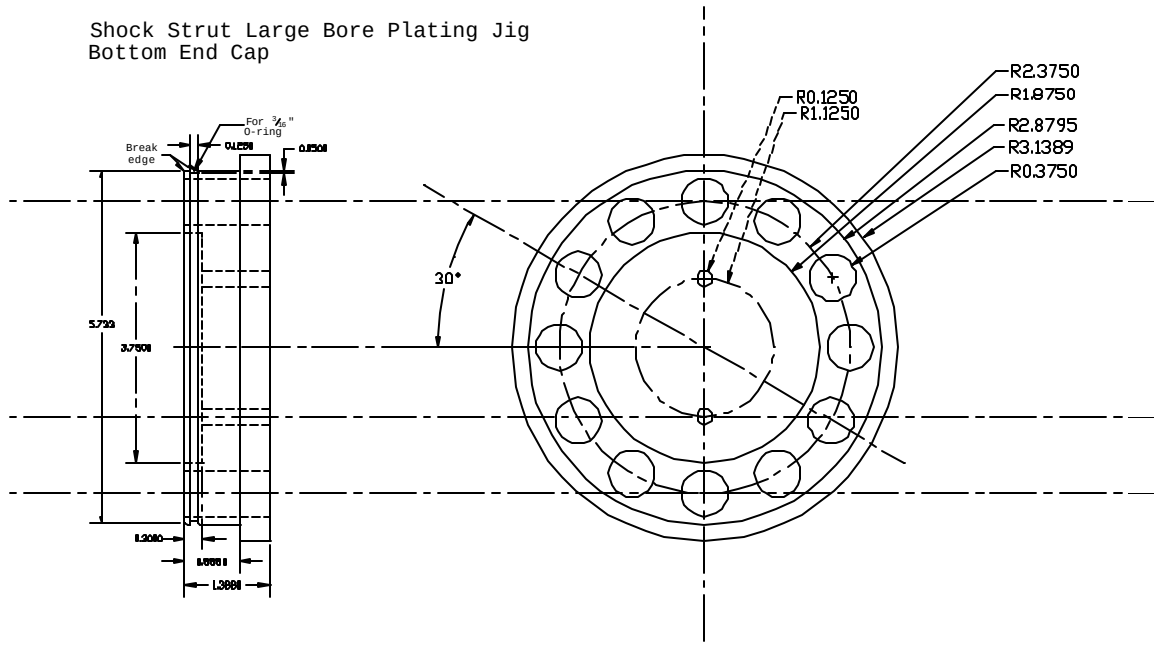

(b)

Figure 5-20 Schematic of the top (a) and bottom (b) end cap used to secure and centre the anode basket in the shock strut component of a landing gear assembly.

Figure 5-21 shows the shock strut of the landing gear component after coating with approximately 0.002" of nanocrystalline Co 2-3wt%P. The coating was found to be free of pits, cracks, and or pores and was uniform throughout.

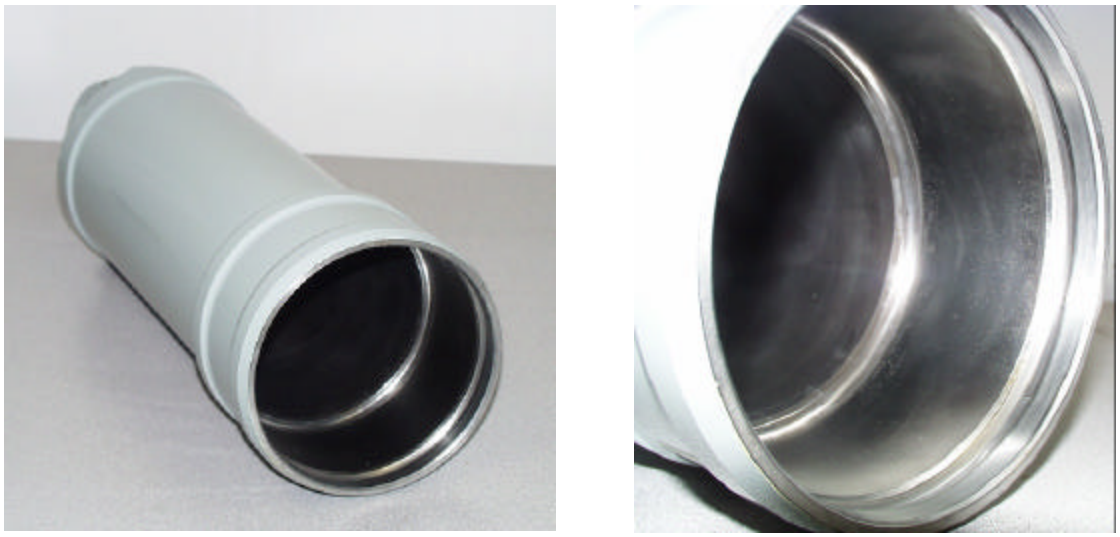

Figure 5-21 The shock strut of a landing gear component (provided courtesy of Messy-Dowty Aerospace) after coating the bottom 2¼" section of the internal diameter with 0.002" of nanocrystalline Co 2-3wt%P.

6.0 SUMMARY

Table 6-1 summarizes the process and properties data of the nanocrystalline Co-P alloy system and compares them with that of hard chrome plating.

Table 6-1 Overall nanocrystalline Co-alloy process and property summary compared with that of hard chrome

PROCESS DATA SUMMARY			
		Nano Co-P Alloy	**Hard Chrome**
Bath Chemistry		Co 2-twt%P ($CoCl_2$ / H_3PO_4 / H_3PO_3)	Cr ($CrO3$ / SO_4^{2-})
Efficiency		85-95%	15-35%
Deposition Rate		Up to 8 mil per hour	Up to 1.6 mil per hour
Thickness		Demonstrated up to 0.020”	Typically <0.005”
As-Deposited Appearance		Pit / Pore Free	Microcracked
Microstructure		Nanocrystalline (avg. g.s.=8-15nm)	-
Relative Process Cost		1.3	1.0
Emission Analysis		Below OSHA limits	Cr^{+6}
PROPERTY DATA SUMMARY			
		Nanocrystalline Co-P	**Hard Chrome**
Hardness	*As-Deposited*	600-700 VHN	800-1200 VHN
	HT @ 250°C	700-800 VHN	-
	HT @ 400°C	1000-1200 VHN	-
Ductility		2-7% Elongation	<0.1%
Thermal Stability		400°C	-
Wear	*Abrasive (Taber)*	27 mg/1000cycles (CS-17)	3.2 mg/1000cycles (CS-17)
		11 mg/1000cycles (CS-10)	1.0 mg/1000cycles (CS-10)
	Adhesive (Pin-on-disk)	5-6 x 10^{-6} mm^3/Nm (Alumina Ball on Nano Co-P Disk)	9-11 x 10^{-6} mm^3/Nm (Alumina Ball on Nano Co-P Disk)
Corrosion	*Salt Spray*	Protection Rating 8 @ 1000 hours	Protection Rating 2 @ 1000 hours
	Poteniodynamic	0.1-1 mpy	0.01 mpy
Internal Stress		10-15 ksi (Tensile)	Cracked – Exceeds cohesive strength
Hydrogen Embrittlement		None	Yes – min bake 24 hrs
Fatigue		Retesting Required	Fatigue Debit

7.0 REFERENCES

1 US Patent No. 5,352,266 Oct.4, 1994

2 US Patent No. 5,433,797 July 18, 1995

3 MIL-C-7460A NOT 1 (March 19, 1993).

4 DOD-STD-2182 (January 29, 1985).

5 MIL-P-6871 (2) (July 27, 1955).

6 MIL-P-19419A (August 21, 1989).

7 D.T. Gawne et al. J.Vac. Sci. Tech., A3 (6), 2334 (1985); Tribology International, 17, 123 (1992).

8 UK Chromium Plating Regulations 1931 (amended in 1973), HMSO (1073).

9 Boyer, H.E. and Gall, T.L. (eds), Metals Handbook, ASM, Metals Park, Ohio (1985)

10 J.K. Dennis and T.E. Such 'Nickel and Chromium Plating' Third Edition Woodhead Publishing Ltd., Cambridge, UK (1993).

11 US Patent No. 5,352,266 Oct.4, 1994

12 US Patent No. 5,433,797 July 18, 1995

13 Cullity, B.D., Elements of X-Ray Diffraction, 2nd Ed., Addison-Wesley Publishing Co, Don Mills, Ontario (1978)

14 Baker, H., ASM Handbook, Vol. 3 - Alloy Phase Diagrams, ASM International, Materials Park, Ohio (1992)

15 G. McMahon and U. Erb, Microstr. Sci, **17**, 447 (1989)

16 G. McMahon and U. Erb, J. Mat. Sci. Lett., **8**, 865 (1989)

17 D. Osmola, E. Renaud, U. Erb, L. Wong, G. Palumbo and K. T. Aust, Mat. Res. Soc. Symp. Proc., **286**, 161 (1993)

18 A. M. Alfantazi and U. Erb, J. Mat. Sci. Lett., **15**, 1361 (1996)

19 S. Wang, Ph.D. Thesis, Queen's University, Kingston, Ontario, Canada (1997)

20 Erb, U., Palumbo, G. and Aust, K.T., Proc. of the NATO Advanced Research Workshop on Nanostructured Films and Coatings, Santorini, Greece, eds. Chow, G-M, Ovid'ko, I.A. and Tsakalakos, T., Kluwer Academic Publishers, Boston (2000)

21 Karimpoor, A., Erb, U., Aust, K.T., Wang, Z. and Palumbo, G., Mat. Sci. Forum, **386-388**, 415 (2002)

[22] Osmola, D., Nolan, P., Erb, U., Palumbo, G. and Aust, K.T., Phys. Stat. Sol. (a) **131**, 569 (1992)

[23] D.H. Jeong, F. Gonzalez, G. Palumbo, K.T Aust and U. Erb, Scripta Mat., **44**, 493 (2001)

[24] B. Stein, "A Practical Guide to Understanding, Measuring and Controlling Stress in Electroformed Metals, *Paper presented at the AESF Electroforming Symposium, March 27-29, 1996, Las Vegas, NV*"